Modification of Structural and Luminescence Properties of Graphene Quantum Dots by Gamma Irradiation and their Application in a Photodynamic Therapy

Journal:	*ACS Applied Materials & Interfaces*
Manuscript ID	am-2015-082266.R1
Manuscript Type:	Article
Date Submitted by the Author:	30-Oct-2015
Complete List of Authors:	Jovanovic, Svetlana; Vinca Institute of Nuclear Sciences, Laboratory for Radiation Chemistry and Physics Syrgiannis, Zois; University of Trieste, Department of Chemical and Pharmaceutical Sciences, INSTM, Center of Excellence for Nanostructured Materials (CENMAT) Markovic, Zoran; Vinca Institute of Nuclear Sciences, Laboratory for Radiation Chemistry and Physics Bonasera, Aurelio ; Humboldt-Universität zu Berlin, Institut für Chemie Kepic, Dejan; Vinca Institute of Nuclear Sciences, Laboratory for Radiation Chemistry and Physics Budimir, Milica; Vinca Institute of Nuclear Sciences, Laboratory for Radiation Chemistry and Physics Milivojevic, Dusan; Vinca Institute of Nuclear Sciences, Laboratory for Radiation Chemistry and Physics Spasojevic, Vuk; Vinca Institute of Nuclear Sciences Dramicanin, Miroslav; Vinca Institute of Nuclear Sciences, Laboratory for Radiation Chemistry and Physics Pavlović, Vladimir ; Faculty of Agriculture Todorovic Markovic, Biljana; Vinca Institute of Nuclear Sciences, Laboratory for Radiation Chemistry and Physics

Modification of Structural and Luminescence Properties of Graphene Quantum Dots by Gamma Irradiation and their Application in a Photodynamic Therapy

Svetlana P. Jovanović,[*,§] *Zois Syrgiannis,*[‖] *Zoran M. Marković,*[§] *Aurelio Bonasera,* [‖,†] *Dejan P. Kepić,*[§] *Milica D. Budimir,*[§] *Dušan D. Milivojević,*[§] *Vuk D. Spasojević,*[§] *Miroslav D. Dramićanin,*[§] *Vladimir B. Pavlović,*[‡] *Biljana M. Todorović Marković*[§]

[§] Vinča Institute of Nuclear Sciences, P.O. Box 522, University of Belgrade, Mike Petrovica Alasa 12-14, 11001 Belgrade, Serbia

[‖] Department of Chemical and Pharmaceutical Sciences, INSTM, Center of Excellence for Nanostructured Materials (CENMAT), University of Trieste, via L. Giorgieri 1, 34127 Trieste, Italy

[‡]Faculty of Agriculture, P.O.B. 127, University of Belgrade, Nemanjina 6, 11080 Zemun, Serbia

KEYWORDS. Graphene quantum dots, gamma irradiation, photoluminescence, quantum yield, photodynamic therapy

ABSTRACT

Herein, the ability of gamma irradiation to enhance the photoluminescence properties of graphene quantum dots (GQDs) was investigated. Different doses of γ-irradiation were used on GQDs to examine the way in which their structure and optical properties can be affected. The photoluminescence quantum yield was increased 6 times for the GQDs irradiated with high doses compared to the non-irradiated material. Both photoluminescence lifetime and values of optical band gap were increased with the dose of applied gamma irradiation.

In addition, the exploitation of the gamma irradiated GQDs as photosensitizers was examined by monitoring the production of singlet oxygen under UV illumination. The main outcome was that the GQDs irradiated at lower doses act as better photoproducers than the ones irradiated at higher doses. These results corroborate that the structural changes caused by gamma irradiation have a direct impact on GQD ability to produce singlet oxygen and their photostability under prolonged UV illumination. This makes low dose irradiated GQDs promising candidates for photodynamic therapy.

1. Introduction

Graphene quantum dots (GQDs) are the newest 0D carbon-based fluorescent nanomaterials with diameter less than 100 nm.[1-3] In these nanomaterials, the contained carbon atoms are sp^2-hybridized indicating that their inner core is characterized by π-conjugated systems. Their most important characteristic is their semiconducting character, represented by a tunable energy band gap, usually less than 1.5 eV.[4-6] Because of this, they possess extraordinary optical and electric properties which distinguish them from other semiconducting quantum dots. Additionally, they have very strong photoluminescence in the visible part of the spectrum and a high resistance to

photobleaching.[3, 7-9] Also, the high charge mobility and tunable conductance make them an ideal material for electronic biosensors.[6]

The synthesis of GQDs can be achieved in two radically different approaches: bottom-up oxidative condensation reactions and top-down cutting of graphene-based materials. Regarding the bottom-up approach, GQDs are being synthesized from small carbon precursors such as citric acid,[3, 10-11] L-glutamic acid,[12] adenosine triphosphate[13] or polycyclic aromatic hydrocarbons.[14] On the contrary, top-down synthesis is based on oxidative cutting of graphene materials: hydrothermal cutting of graphene,[7, 15] carbon nanotubes,[16-17] fullerenes[18] as well as electrochemical methods [1, 19-21]. A convenient and low cost top-down method is the electrochemical one, where a graphite electrode is used as a starting material. In this study, we used the electrochemical method to obtain GQDs for possible application in photodynamic therapy.

One of GQDs' main characteristics is high solubility in water,[22] which together with low toxicity and biocompatibility[23] presents them as an attractive material for biological applications: *in vitro* and *in vivo* cell imaging,[12, 24] targeted drug delivery[25] and photodynamic therapy[26-28].

Photodynamic therapy (PDT) is a non-invasive treatment for selective cancer cell destruction and in antimicrobial therapy.[29-30] This approach demands the co-localization of oxygen molecules, light and photosensitizers (PS) which will convert oxygen into reactive singlet oxygen ($^1O_2$) and cause photocytotoxicity. Our recent study showed that GQDs upon blue light illumination generate reactive $^1O_2$ and kill human glioma cells.[26] Ge *et al.* demonstrated high capability of GQDs to generate $^1O_2$ (with quantum yield ~1.3) and their high efficiency as photosensitizers simultaneously allowing the imaging.[28]

According to our previous results, gamma irradiation showed a great potential for modification of carbon based nanomaterials, such as carbon nanotubes and graphene. The changes that occurred after the irradiation are mainly affecting the functional groups.[31-34] Based on these results, our investigation was extended on GQDs. More specifically, we explored if their photoluminescence properties can be improved by gamma irradiation and their consequent potential for use in PDT. In this work, pristine GQDs were synthesized from graphite rods through the electrochemical procedure. These GQDs were irradiated with different doses of gamma irradiation. The irradiation is performed on GQDs dispersed in a mixture of water and isopropyl alcohol, in order to create a reductive environment. It has already been reported, that the use of classical chemical reduction with hydrazine, can lead to enhancement of the photoluminescence of GQDs.[35] Hence, we chose a medium in which reducing agents are dominantly formed (hydrogen, electrons and isopropyl radicals) upon gamma irradiation.[36] Different characterization techniques were used for the study of structural, optical and particularly photoluminescence properties. The gamma irradiated GQDs reached photoluminescence quantum yield six times higher than the pristine ones. The final objective of this work was to examine the ability of pristine and irradiated GQDs to act as photosensitizers. Their efficiency as an agent for PDT was investigated by following the real time singlet oxygen production.

2. Experimental

2.1. Synthesis of GQDs

GQDs were synthesized by following the previously reported electrochemical procedure.[37] Spectroscopic graphite rods were used both as anode and cathode. A dispersion of NaOH in

ethanol (EtOH) was used (in a concentration of 3%) as an electrolyte, and the current intensity was set to 20 mA. Afterwards, the EtOH solution of GQDs was neutralized with HCl, and then NaCl was flocculated and separated from the solution by filtration. Ethanol was evaporated and finally the solid was collected. GQDs were further purified by dialysis (molecular weight cut-off 3500 Da) for 1 day.

The pristine GQDs were then exposed to different doses of gamma irradiation. Dispersions for irradiation were prepared by sonication of GQDs in water, in a concentration of 1 mg/ml. Isopropyl alcohol was gradually added to the dispersion, until the final concentration was reached (4%). Prepared samples were irradiated by gamma ray flux from ^{60}Co nuclide with the photon energy of 1.3 MeV (Centre of Irradiation, Vinča Institute of Nuclear Sciences) at a dose rate of 18.6 kGyh^{-1}. Samples were exposed to the source of gamma irradiation absorbing the doses of 20, 50, 100 and 200 kGy (in the further text, samples are labeled as $_{20}\gamma$-GQDs, $_{50}\gamma$-GQDs, $_{100}\gamma$-GQDs and $_{200}\gamma$-GQDs, respectively). Irradiation treatment was followed by evaporation to dryness. Then, MiliQ water was added and again evaporated. Non-irradiated GQDs are named as pristine GQDs (*p*-GQDs). Details of methods used for GQDs characterization are described in the "Equipment" section (**Supporting Information**).

3. Results and discussion

3.1. Surface morphology and structural characterization of GQDs

AFM was used to investigate the morphology of GQDs as well as their height and diameter distribution. Figure 1 shows representative large-scale AFM images and histograms of both diameter and height distribution for all GQDs samples. The results of AFM image analysis are presented in Table 1.

Table 1. The values of average real diameter and average height of GQDs, in nm.

Sample	Diameter	Height
p-GQDs	24.0	1.1
$_{20}\gamma$-GQDs	27.3	3.3
$_{50}\gamma$-GQDs	18.2	3.0
$_{100}\gamma$-GQDs	20.7	2.6
$_{200}\gamma$-GQDs	23.2	2.9

Considering that single layer graphene quantum dots have thicknesses between 0.7 and 1 nm measured by AFM,[1, 38] we concluded that *p*-GQD are single layer GQDs. According to AFM measurements, the first change noticed in the GQDs after gamma irradiation is in the number of layers: two or three graphene layers instead of the monolayer noticed for pristine GQDs.

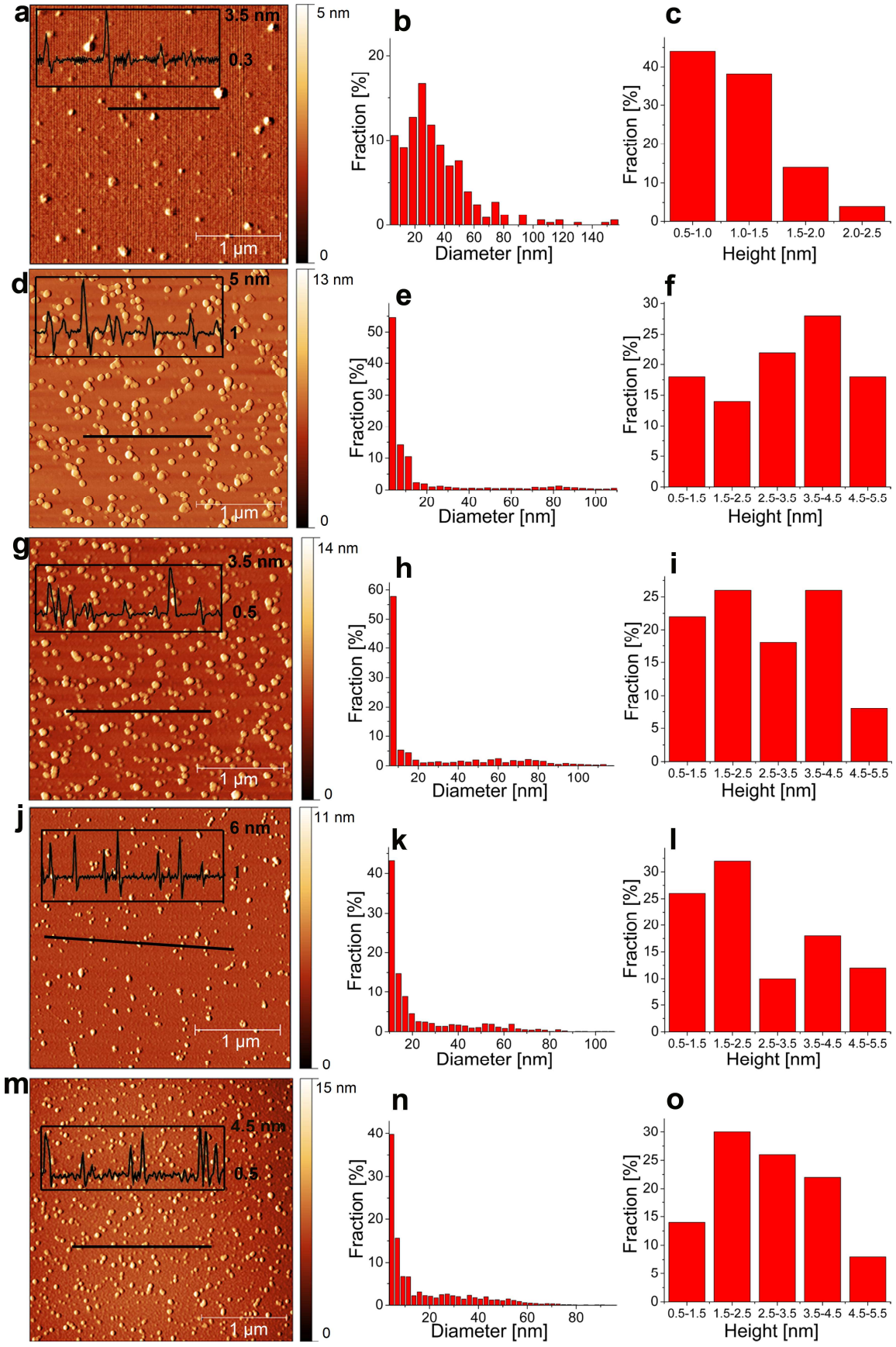
a
3.5 nm
0.3
1 µm
5 nm
0
b
Fraction [%]
Diameter [nm]
c
Fraction [%]
0.5-1.0
1.0-1.5
1.5-2.0
2.0-2.5
Height [nm]
d
5 nm
1
1 µm
13 nm
0
e
Fraction [%]
Diameter [nm]
f
Fraction [%]
0.5-1.5
1.5-2.5
2.5-3.5
3.5-4.5
4.5-5.5
Height [nm]
g
3.5 nm
0.5
1 µm
14 nm
0
h
Fraction [%]
Diameter [nm]
i
Fraction [%]
Height [nm]
j
6 nm
1
1 µm
11 nm
0
k
Fraction [%]
Diameter [nm]
l
Fraction [%]
Height [nm]
m
4.5 nm
0.5
1 µm
15 nm
0
n
Fraction [%]
Diameter [nm]
o
Fraction [%]
Height [nm]

Figure 1.AFM images and histograms of diameter and height distribution for *p*-GQDs (a, b, c), $_{20}$γ-GQDs (d, e, f), $_{50}$γ-GQDs (g, h, i), $_{100}$γ-GQDs (j, k, l) and $_{200}$γ-GQDs (m, n, o).

The lateral size of GQDs is additionally investigated with transmission electron microscopy (TEM). These micrographs are shown in figure S1 (**Supporting Information**). The representative TEM micrograph of *p*-GQDs (figure S1, a) shows two GQDs with the lateral size of 32.0 and 20.4 nm. For $_{20}$γ-GQDs, an average TEM micrograph shows that the dots size is 25.6 nm, while the size of $_{50}$γ-GQDs varies from 17.8 to 9.8 nm. As for $_{100}$γ-GQDs, the TEM micrograph shows the dot size of 20.1 nm. The TEM micrograph of $_{200}$γ-GQDs sample indicates that the average size of GQDs is 22.4 nm. These results are in good agreement with the results obtained from AFM analysis.

Overall AFM and TEM analyses show that, by varying the dose of irradiation, both the diameter and the number of graphene layers in GQDs could be affected. The highest decrease in GQDs diameter was noticed for gamma irradiation at 50 kGy (average of 18 nm). Also there is a significant narrowing of the diameter distribution. Further increase in irradiation dose (100 and 200 kGy) has a smaller effect on the diameter of GQDs, but again causes the narrowing of the diameter distribution in both samples. Moreover, all doses caused the increase in the number of graphene layers in GQD. This phenomenon could be explained by a lower content of carboxyl groups and at the same time an increase in the sp^2 character of GQDs[38] which can yield to the merging of "graphene" sheets upon irradiation.[39]

The next step was to examine the changes in the chemical composition of the GQDs. For this reason FT-IR was used to identify the functional groups of pristine and gamma irradiated GQDs (figure 2). FT-IR spectrum of pristine GQDs (figure 2, a) shows peaks near 3000 and 1572 cm^{-1}

associated to the C=C stretching of graphite, which indicates the presence of sp^2-hybridized graphitic cores.[40] Peaks at 1045 and 2974 cm^{-1} stem from C−O vibrations of alkoxy groups. The emerging peaks at 1011 cm^{-1} and 1365 cm^{-1} are related to the vibration of C−O bonds and symmetric stretching of carboxyl groups, respectively. The band at 1700 cm^{-1} stems from vibration of carbonyl functional group in COOH. Peak at 2697 cm^{-1} stems from C=O vibration of aromatic aldehyde. Two peaks at 2781 and 2933 cm^{-1} are associated to stretching vibrations of −CH and $-CH_2$ groups. A broad band at 3400 cm^{-1} is related to the vibrations of O−H bonds.

As for gamma irradiated GQDs, same bands are identified in FT-IR spectra as in the spectrum of *p*-GQDs.

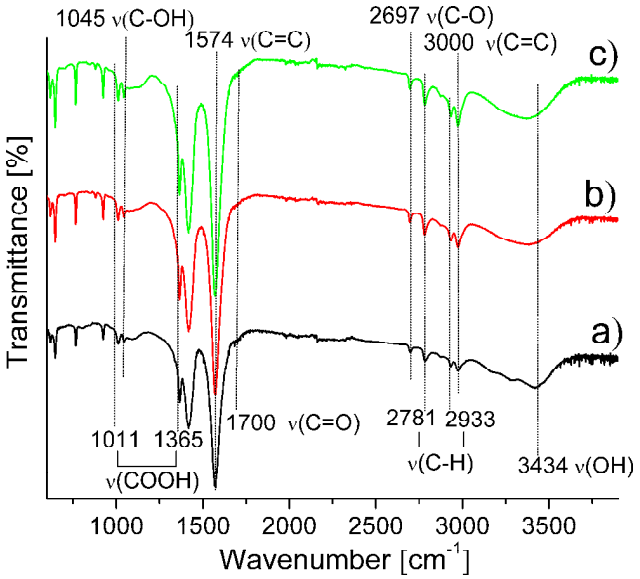

Figure 2.FT-IR spectra of *p*-GQDs (a), $_{20}$γ-GQDs (b) and $_{200}$γ-GQDs (c).

FT-IR spectra analysis was used for identification of polar functional groups: carbonyl, carboxylic and hydroxyl. Such functional moieties are responsible for their high solubility in water and polar organic solvents. On the other hand, π-conjugated core is preserved after gamma

irradiation. At this point, we could not conclude if gamma irradiation has any effect on the type of the functional groups in the structure of GQDs.

Consequently, elemental analysis (EA) was used for further exploring the effect of the gamma irradiation on the changes that took place on the atomic scale. These results are shown in Table 2, in mass percentage of each element. The EA of GQDs shows the increase in oxygen content for all gamma irradiated samples. The highest increase is noticed for GQDs irradiated at doses of 20 and 50 kGy, where oxygen content increased for 9.2 % compared to *p*-GQDs.

Table 2. The elemental analysis of graphene quantum dots.

Sample	N %	C %	H %	O %
p-GQDs	0.0	56.0	8.1	35.9
$_{20}\gamma$-GQDs	0.0	43.8	11.1	45.1
$_{50}\gamma$-GQDs	0.0	45.0	9.9	45.1
$_{100}\gamma$-GQDs	0.0	46.8	9.3	43.9
$_{200}\gamma$-GQDs	0.0	47.0	10.5	42.5

From the FT-IR and the EA analyses we can conclude that there were quantitative changes in the amount of each atom, but no qualitative changes in the functional groups of GQDs.

UV-Vis spectra of pristine and gamma irradiated GQDs are presented in figure 3. All the spectra show the highest absorbance in the UV region. Absorbance values exponentially decrease versus the higher wavelengths, which is in agreement with previous reports.[1]

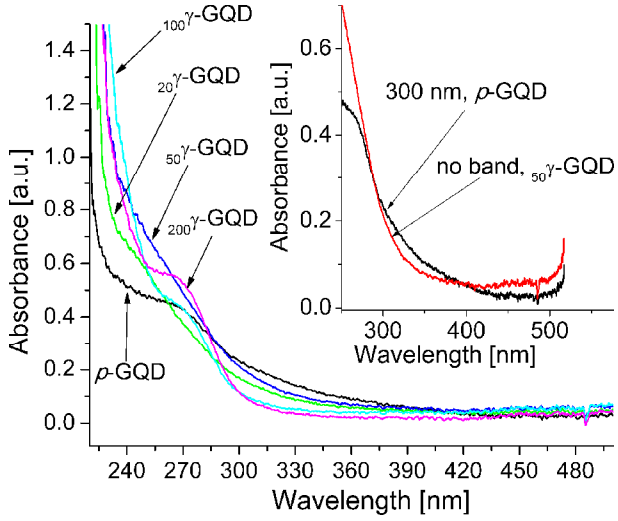

Figure 3.UV-Vis spectra of pristine and irradiated GQDs. In the upper right corner, an enlargement of UV-Vis spectra of pristine and $_{50}\gamma$-GQDs is shown.

A shoulder absorption peak at 267 nm was noticed for GQDs and this peak was assigned to π-π* transition of sp^2 domains.[23] In figure 3 (the insert in the upper right corner), additional shoulder at 300 nm is observed and it is assigned to n-π* transition of C=O bonds. After gamma irradiation at lower doses (20 and 50 kGy), absorption peaks become broader and blue-shifted to 250 nm, while at higher doses peaks are closer to the position detected for pristine GQDs (at around 270 nm).

Even though the positions of absorption peaks are shifted for $_{20}\gamma$-GQDs and $_{50}\gamma$-GQDs samples, this band is still in the characteristic range for π-π* transition. The position of the absorption band is strongly correlated to the preparation method and oxygen content. It has been already reported that absorbance peaks could be shifted as a result of the variation in carboxyl group content.[41] For gamma irradiated GQDs, bands at around 300 nm were not found. Considering that this band is related to the carbonyl functional group, results suggest that gamma irradiated GQDs have a lower content of these groups.

The structure of GQDs before and after gamma irradiation was additionally investigated by acid-base titrations. The number of carboxyl functional groups was determined by using previously described procedure.[42] For gamma irradiated GQDs, a decrease in the number of acid sites was observed. The amount of acid sites is similar for all irradiated GQDs (figure S2, S**upporting Information**) and it is around 0.14 mmol/g while in the *p*-GQDs this number is almost double (0.25 mmol/g). Consequently, we proved an increase in other type of oxygen containing groups after irradiation, such as carbonyl, ethoxy and hydroxyl.

Considering the results of FT-IR, EA, UV-Vis and acid-base titrations we can conclude that gamma irradiation caused the partial reduction of carboxyl and carbonyl functional groups. But also, this treatment caused a large increase in oxygen and hydrogen content probably by forming new OH groups in the structure of gamma irradiated GQDs.

3.2. Photoluminescence of GQDs

Photoluminescence of *p*-GQDs was investigated at different laser excitation wavelengths: from 328 to 469 nm (figure 4a). GQDs emission spectra are dependent on the laser excitation wavelength; when the excitation wavelength changed from 328 nm to 469 nm, emission wavelength shifted from 425 to 520 nm, respectively. The excitation-dependent PL behavior of GQDs was related to differences in lateral sizes of GQDs in the sample and/or different emissive sites on GQDs.[17, 43] Similar behavior was detected for gamma irradiated GQDs (figures S3-S6, S**upporting Information**). The wide diameter distribution in samples of GQDs, which was confirmed from the AFM analysis, is responsible for their excitation-dependent behavior.

The highest intensities of emission bands were detected for excitation wavelength of 341 nm, thus this laser wavelength was chosen for further examination of GDQs.

Irradiation at a dose of 20 kGy did not cause large changes in the PL intensity of GQDs. The $_{50}\gamma$-GQDs dispersion emits a strong photoluminescence light which is almost 5 times more intense compared to the emission of pristine GQDs (figure 4b). However, further increase of irradiation dose did not cause an increase of PL intensity. The values of PL intensity are around 3 times higher for $_{100}\gamma$-GQDs and $_{200}\gamma$-GQDs compared to *p*-GQDs. Considering the highest recorded photoluminescence and the aforementioned results from FTIR, EA and AFM analyses, we concluded that both high content of −OH groups and quantum confinement effect are of high importance in the mechanism of $_{50}\gamma$-GQD photoluminescence.

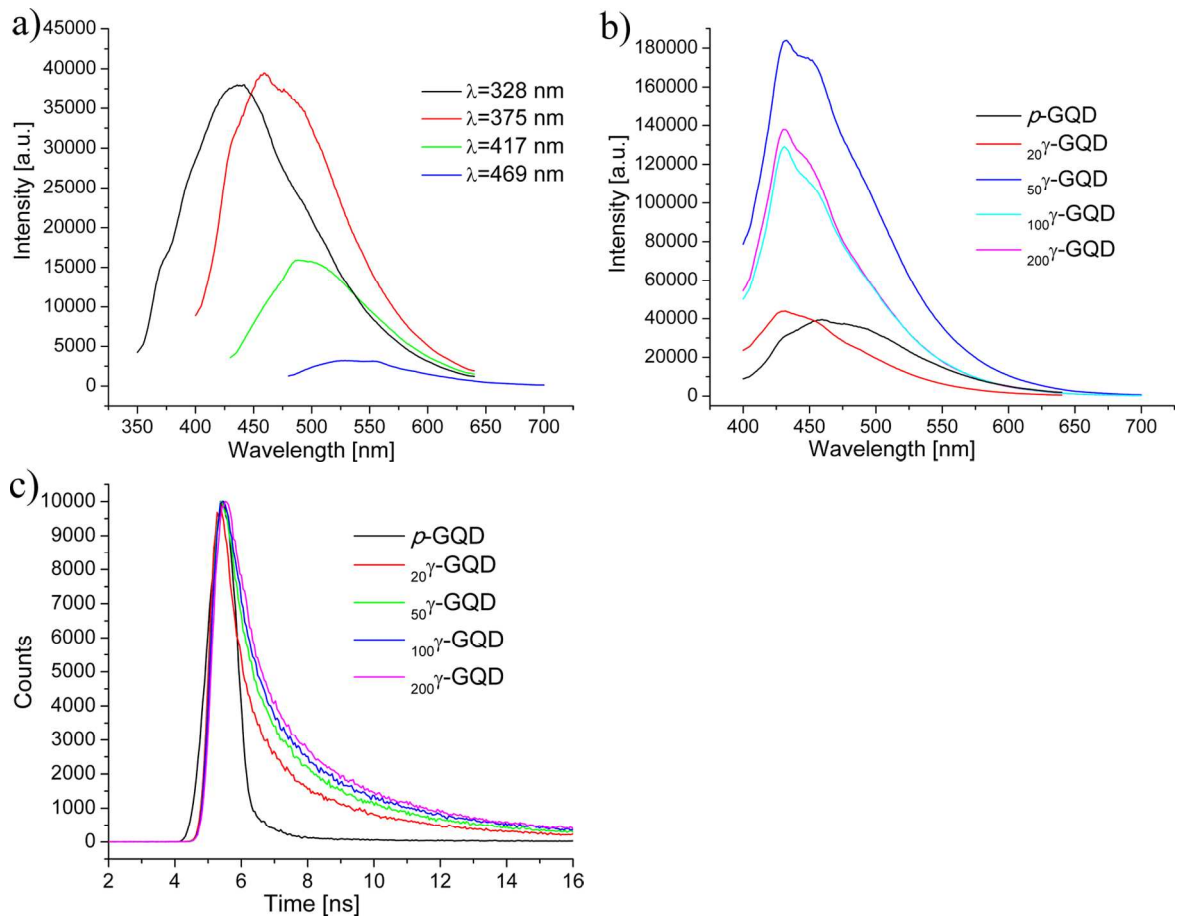

Figure 4.Photoluminescence spectra of *p*-GQDs at different laser excitation wavelengths (a); photoluminescence spectra of pristine and GQDs irradiated at dose of 20, 50, 100 and 200 kGy

measured at the pulsed laser excitation at 341 nm (b); PL decay curves for pristine and gamma irradiated GQDs (λ_{exc} = 341 nm) (c).

The emission bands are blue-shifted, from 460 to around 430 nm, for all gamma irradiated GQDs (Table 3). The shifts in emission spectra of different GQDs are the result of changes in the defect structure, edge configuration, size or shape.[44-46] Zhu *et al.* showed that green PL of GQDs can be changed into blue by changing carbonyl and epoxy groups into −OH, thus non-radiative process were blocked and the integrity of π-conjugated system is enhanced.[47] Furthermore, Xu *et al.* suggested that blue PL results from the localization of discrete energy levels inside the sp^2 carbon domains due to quantum confinement.[48] With particular regard for gamma irradiated GQDs, the blue shift of the PL band is probably related to the increase in OH functional groups content, located at their edges, and partial restoring of sp^2 carbon domains in all gamma irradiated GQDs.

Table 3.PL band positions and intensities for pristine and gamma irradiated GQDs, and the values of lifetime components.

Sample	Emission band (nm)	Intensity (a.u.)	Lifetime components (ns)		
			τ_1 (faster)	τ_2 (slower)	τ_{aver} (average)
p-GQDs	460	40552	0.49	/	0.49
$_{20}\gamma$-GQDs	430	45515	0.59	2.96	0.59
$_{50}\gamma$-GQDs	432	188590	0.90	2.32	0.94
$_{100}\gamma$-GQDs	429	134886	0.95	2.99	0.98
$_{200}\gamma$-GQDs	431	143463	0.99	3.27	1.04

The photoluminescence decay profiles were measured at 341 nm excitation wavelength, and showed in figure 4c. For *p*-GQDs, a single exponential lifetime decay was noticed, which suggests that the origin of photoluminescence is one single species.[49] All curves of gamma irradiated GQDs are fitted using bi-exponential function to calculate the lifetimes, which suggests that two relaxation pathways are responsible for the PL exciton decay. For fitting, the function: $I(t) = A_1e^{t/\tau 1} + A_2e^{t/\tau 2}$ was used, where A_1 and A_2 are the percentage of contribution while τ_1 and τ_2 are faster and slower life-time components, respectively. An average life-time is defined by these parameters and can be calculated with the function: $\tau_{average} = A_1\tau_1 + A_2\tau_2/(A_1+A_2)$.[48]

Table 3 summarizes the results of life-time component analysis. As we can see, gamma irradiated GQDs show the two life-time components of long and short-lived excited species; both components and average life-time depend on gamma irradiation dose. Previous reports showed that for single-layer GQDs, their PL decay process consists of both radiative electron-hole recombination and non-radiative carrier relaxation into other emissive or non-emissive states.[48] When multiple layers of sp^2 domains are stacked together, in a case of multi-layer GQDs, one additional channel for the non-radiative decay of carriers would be opened due to possible interactions between neighboring layers. In our case, life-time increases with irradiation dose due to the increase in the number of graphene layers, as AFM imaging showed.

The relative photoluminescence quantum yields (φ) of *p*- and gamma irradiated GQDs were measured using quinine sulfate as a reference. These results are shown in Table S1 (**Supporting Information**). With the increase of irradiation dose, φ also increases. For $_{200}$γ-GQDs, φ is six times higher than for *p*-GQDs (4.3% and 0.7%, respectively).

The electronic properties of materials were studied by measuring their band gap energy (E_g) through obtaining diffuse reflectance spectra (DRS).[50-51] In figure S7 (**Supporting Information**), DRS for GQDs before and after gamma irradiation are shown. Significant difference can be seen in the spectrum of *p*-GQDs compared to spectra of GQDs irradiated at lower doses (20 and 50 kGy) and GQDs irradiated at high doses (100 and 200 kGy). These differences are attributed to the structural changes caused by irradiation treatment, as we previously discussed. Spectra displayed in figure S7 are used to calculate band gap energy for each GQD sample.

To analyze the band gap, the Kubelka-Munk remission function was used ($F(R)=(1-R)^2/2R$).[52] Figures S8 (a-e) (**Supporting Information**) show the determination of E_g values for pristine and gamma irradiated GQDs. For pristine GQDs, band gap is 1.99 eV, while for GQDs irradiated with lower dose, values of optical band gaps are higher than for pristine: for $_{20}\gamma$-GQDs samples it is 2.12 and for $_{50}\gamma$-GQDs ones is 2.16 eV. Further increase of this parameter is noticed for GQDs irradiated with higher dose (for $_{100}\gamma$-GQDs sample it is 2.27, and for $_{200}\gamma$-GQDs it is 2.29 eV).

Figure S8 (f) shows the dependence between E_g values and the applied gamma irradiation dose. These results suggest that with the irradiation dose, E_g values also increased. At higher doses (100 and 200 kGy) the value of E_g reaches maximum values. Two factors can affect E_g, the lowering of C-sp^2 or the increase of O-containing groups.[50] Based on EA, at the doses of 20 and 50 kGy the increase in oxygen groups is dominant. However, at higher doses, further changes in GQDs structure caused additional increase in E_g value. The formation of interlayer covalent bonding between C-sp^2 cores of GQDs takes place at these doses [39] and is responsible for further increase of E_g value.

3.2. EPR of GQDs

In order to understand the role of gamma irradiation in the modulation of GQD π-electron structure, EPR analysis was carried out. The spectra are shown in figure 5 and the parameters obtained from EPR spectra: g factor, A/B ratio, ΔHpp and T_2 are presented in Table 4.[53] All EPR spectra show a single narrow and symmetric EPR signal of Lorentzian shape. These sorts of signals are evidence of the existence of free electrons in all GQDs samples.

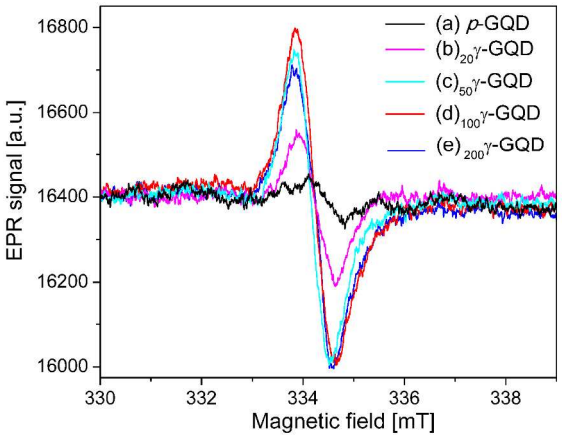

Figure 5.EPR spectra of *p*-GQDs (a), $_{20}$γ-GQDs (b), $_{50}$γ-GQDs (c), $_{100}$γ-GQDs (d) and $_{200}$γ-GQDs (e).

The g factor value is related to the molecular motion, symmetry of ions and paramagnetic properties of material.[54] For *p*-GQDs, g factor is ≈ 2.0029. The values of g factor are nearly constant for all gamma irradiated GQDs (g = 2.0031). For electron pair near a carbon-hydrogen bond, the value of g factor is 2.0031 and it suggests that in our samples spins are delocalized over a few carbon atoms in an aromatic ring.

The parameter A/B ratio is related to the asymmetric nature of EPR signals. We observed significant changes in A/B ratio upon gamma irradiation: the values of this parameter vary from

1.309 for *p*-GQDs to 0.467 for $_{20}\gamma$-GQDs. The A/B ratio depends on the concentration of electrons localized in the conduction band. If the value of A/B ratio is around or below 1 it indicates an insulator, while higher values (up to 9) were observed in metallic samples.[55] The lower ratio measured in gamma irradiated samples could suggest a larger population of localized paramagnetic electrons at zigzag edges than in the sample of *p*-GQDs.

The interaction of spins with their environment and their motion are associated with the EPR signal width. The parameter ΔH_{pp} is called peak-to-peak linewidth and its value has decreased after gamma irradiation at all doses.[56] On the contrary, T_2 parameter describes spin-spin relaxation time and its values have increased for all gamma irradiated GQDs. The width of an EPR signal depends on the extent of delocalization of unpaired electrons. The results presented in Table 4 suggest that gamma irradiation caused the enhancement of electron mobility in GQDs. Increased spin mobility found in gamma irradiated GQDs could be explained by a greater delocalized π-cloud. Namely, the π-cloud in the core of *p*-GQDs is disrupted by hydroxyl and epoxy functional groups. After gamma irradiation in mixture of water and IPA, these functional groups have been partially reduced and thus the delocalization of π electrons along GQDs core is extended.

The most significant changes in values of parameters A/B, ΔH_{pp} and T_2 are measured for $_{20}\gamma$-GQDs. Considering the highest percentage of oxygen in this sample, it is possible that groups such as - OH, -O, -CO, -C=O bonded to graphene core edges, can be responsible for reduced peak-to-peak linewidth and the formation of EPR radicals.[57] The additional factor is a possibility that gamma irradiation, at the lowest dose, caused a small increase in the content of the zigzag edge carbon atoms.[58] The contribution of both factors results in a large change in all three above mentioned parameters.

Table 4.EPR parameters for *p*-GQDs and gamma irradiated GQDs: g factor, parameter of peak-peak asymmetric nature (A/B), peak-to-peak linewidth (ΔH_{pp}) and spin-spin relaxation time (T_2).

Sample	g factor	A/B	ΔH_{pp} (G)	T_2 (x 10^{-9} s)
p-GQDs	2.0029	1.309	5.14	6.29
$_{20}\gamma$-GQDs	2.0031	0.467	1.64	19.72
$_{50}\gamma$-GQDs	2.0031	0.880	2.79	11.59
$_{100}\gamma$-GQDs	2.0031	0.836	3.29	9.83
$_{200}\gamma$-GQDs	2.0031	1.107	3.73	8.67

The intensity, obtained as a double integral of the EPR spectrum, is proportional to the number of EPR scattering centers - number of localized spins at zigzag edges of graphene in this case. Thus, figure 5 shows that the number of defect edge states increases with irradiation dose and reaches the maximum at 100 kGy.

3.3. GQDs as a photosensitizer

The ability of GQD solutions to produce singlet oxygen with and without photo-excitation was examined. The samples of pristine and gamma irradiated GQDs were also recorded with EPR in presence of 2,2,6,6-tetramethylpiperidine (TEMP) which was used as a spin trap agent. The molecules of TEMP selectively react with singlet oxygen ($^1O_2$) and form the stable product, 2,2,6,6-tetramethylpiperidine-1-oxyl (TEMPO), which shows a characteristic EPR signal.[59-60]

In figure 6, EPR spectra of TEMP ethanol solution in dark (indicated “TEMP dark”) and light (indicated “TEMP light”) conditions do not show any signal. By addition of *p*-GQDs in TEMP solution, in dark conditions, three very weak lines are noticed, indicating the TEMPO product formation in low concentration (figure 6, spectrum “TEMP with *p*-GQDs in dark”). But the

illumination for 10 minutes with UV-light (λ > 300 nm), caused considerable changes in EPR signal (figure 6, TEMP + *p*-GQDs in light) consisting of three equally intense lines. This spectrum proves the formation of TEMPO in *p*-GQDs upon illumination and thus their capability to be photosensitizers. EPR spectra of *p*-GQDs and gamma irradiated GQDs in TEMP solution are recorded after 1, 10 and 20 minutes of UV-light illumination (figure S9, **Supporting Information**). These spectra show that intensities of EPR signal increase with time of illumination, for all GQDs. The highest intensities of EPR signals are observed in $_{20}$γ-GQDs and $_{50}$γ-GQDs samples after 20 minutes (figure S9 f, **Supporting Information**).

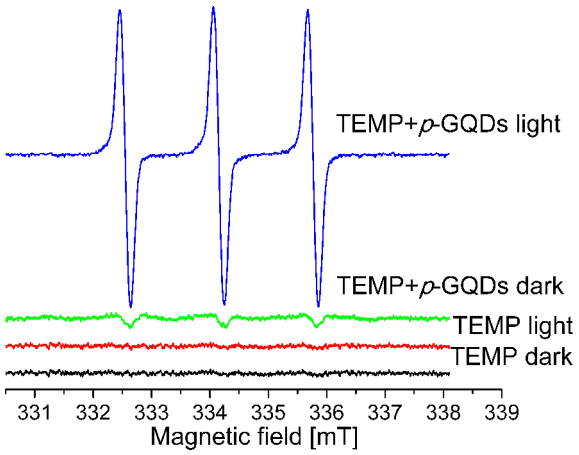

Figure 6.EPR spectra of several experimental conditions: TEMP solution in dark conditions, TEMP solution under UV-light, TEMP with *p*-GQDs in dark conditions and TEMP solution with *p*-GQDs under UV-light.

A time-accumulating EPR spectra of pristine and gamma irradiated GQDs solutions containing TEMP were recorded upon UV illumination for 20 minutes. The concentration of generated $^1O_2$ is calculated by using 2,2-Diphenyl-1-picrylhydrazyl (DPPH) solution as standard. Time dependent $^1O_2$ generation in solutions of GQDs samples upon UV illumination is showed in figure 7a. For *p*-GQDs, the production of $^1O_2$ increases linearly in the first 12 minutes of

illumination, after which it starts to stagnate and fall down. All gamma irradiated samples show linear and continual increase in $^1O_2$ generation with time. The highest concentrations of $^1O_2$ were detected for GQDs irradiated at doses of 20 and 50 kGy after 20 minutes. Under these conditions, pristine and gamma irradiated GQDs showed very different behavior: $^1O_2$ generation for pristine GQDs increases up to 12 minutes after which it falls, while for all gamma irradiated GQDs $^1O_2$ generation increases linearly with time.

The long-term generation of $^1O_2$ upon UV illumination is investigated for pristine and GQDs irradiated at doses of 50 and 100 kGy, figure 7b. For gamma irradiated GQDs, these measurements showed that the concentration of $^1O_2$ was increasing up to the 30th minute and stagnated up to the 45th, after which it was falling down. This trend was continued for 15 minutes (until the 60th minute), after which the concentration of $^1O_2$ again increases for one hour. This behavior is noticed for both $_{50}\gamma$-GQDs and $_{100}\gamma$-GQDs, while for the whole measurement time the concentration of produced $^1O_2$ was higher in the $_{50}\gamma$-GQDs sample. As for *p*-GQDs, it was observed that the concentration of $^1O_2$ reached the saturation, after around 13 minutes of UV illumination and then it was falling.

The oscillations in $^1O_2$ production indicate the dual mechanism of singlet oxygen production by gamma irradiated GQDs under UV illumination. Ge et al. showed that GQDs generate singlet oxygen through a new mechanism named multistate sensitization (MSS).[28] They established that singlet oxygen can be produced in two ways: energy transfer from the excited triplet state (T1) GQDs to O_2 and energy transfer from the excited singlet state (S1) of GQDs to triplet oxygen ($^3O_2$) that leads to $^1O_2$ generation during the S1–T1 intersystem crossing transition.

This two-stage mechanism explains the presence of feedback and the oscillations in singlet oxygen generation in samples of gamma irradiated GQDs (figure 7b). In the stage of increased $^1O_2$ production, both S1 and T1 lead to $^1O_2$ formation, while in the stagnating stage $^1O_2$ is probably produced by S1–T1 intersystem crossing transition, when $^3O_2$ may also lead to $^1O_2$.[28] The lowering in $^1O_2$ production is probably a result of the consumption of dissolved oxygen in the system. The following new increase in $^1O_2$ production started when enough oxygen is diffused in the system. The *p*-GQDs probably underwent photolysis after 13 minutes of UV illumination, which caused stagnation and later decrease in singlet oxygen production.

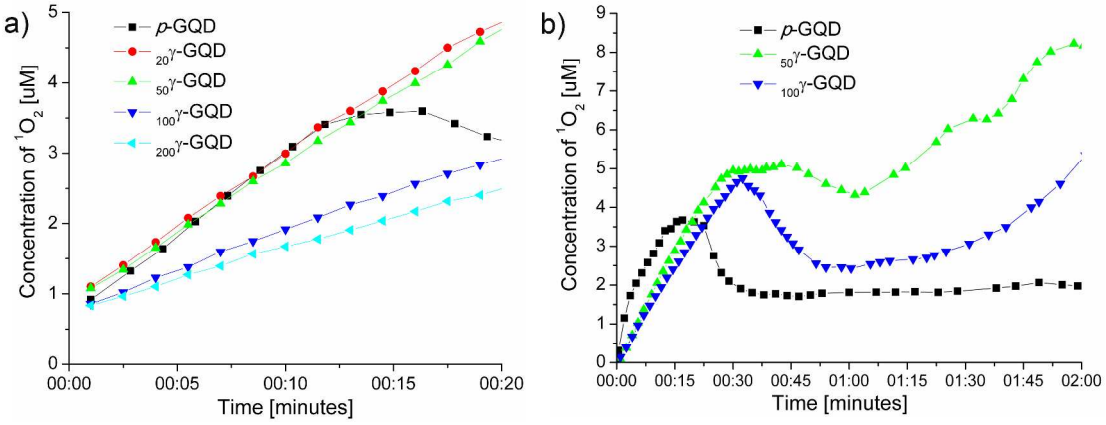

Figure 7.(a) Singlet oxygen formation (measured with TEMPO) as a function of UV illumination time for 20 minutes, in ethanol solution containing *p*-GQDs (-■-), $_{20}$γ-GQDs (-●-), $_{50}$γ-GQDs (-▲-), $_{100}$γ-GQDs (-▼-) and $_{200}$γ-GQDs (-◀-), (b) production of singlet oxygen during two hours of UV illumination for *p*-GQDs (-■-), $_{50}$γ-GQDs (-▲-), $_{100}$γ-GQDs (-▼-).

Singlet oxygen production of GQDs was additionally investigated through an established photochemical procedure, based on the use of 1,3-diphenylisobenzofurane (DPBF) as an efficient quencher of $^1O_2$.[61-64] The results of these measurements are shown in figure S10 (**Supporting Information**). In the figure S10 a), the absorption spectra of DPBF and the GQD

solutions mixed with DPBF are presented. These spectra are recorded immediately after mixing DPBF with GQDs and showed similar intensity for all samples. After eight minutes of UV illumination (figure S10 b, **Supporting Information**), the intensity of the absorption peak located at 415 nm, reduces for the irradiated samples, and is the lowest in the spectrum of $_{50}\gamma$-GQDs. These results confirm the higher production of $^1O_2$ in gamma irradiated GQDs compared to *p*-GQDs.

Considering the capability to generate $^1O_2$ solely upon UV illumination, their high water solubility and low toxicity, GQDs seem to be promising candidates for photosensitizers in PDT. These results show that gamma irradiated GQDs have better stability to photolysis, higher phototoxicity and more stable singlet oxygen generation over time compared to pristine GQDs.

4. Conclusion

In this work, a novel approach to increase the photoluminescence of GQDs is presented. Gamma irradiation is suggested to be a valuable method for the modification of optical properties of GQDs considering low chemical consumption and room temperature conditions. By changing the dose of gamma irradiation, different GQD properties can be modulated: the diameter, structure (specifically oxygen content), photoluminescence intensity, position and lifetime, optical band gap energy as well as singlet oxygen production.

The enhancement of GQDs photoluminescence is the most important result, since it discloses the possibility of real application for graphene quantum dots in bioimaging and photodynamic therapy. By applying gamma irradiation at a dose of 50 kGy, significant improvement of PL properties was observed (PL intensity 4.5 times higher, excited state lifetime two times longer). At this dose, the highest amount of oxygen was detected in the structure of GQDs. The high

capacity of $_{50}\gamma$-GQDs to generate single oxygen upon UV illumination together with high photoluminescence make this sample a promising candidate for *in vitro* and *in vivo* studies as an agent with a dual role as a photosensitizer in PDT and a contrast for imaging.

ASSOCIATED CONTENT

Supporting Information. Materials, equipment, figures S1-S10 and table S1 are discussed in text. This material is available free of charge via the Internet at http://pubs.acs.org.

AUTHOR INFORMATION

Corresponding Author

*Tel +381 11 3408 582, Fax +381 11 344 0 100, E-mail address: svetlanajovanovic@vinca.rs

Present Addresses

† Humboldt-Universität zu Berlin, Institut für Chemie, Brook-Taylor-Straße 2, 12489 Berlin, Germany

Author Contributions

The manuscript was written through contributions of all authors. All authors have given approval to the final version of the manuscript.

ACKNOWLEDGMENT

This research was supported by the Ministry of Education, Science and Technological Development of Republic of Serbia (project no. 172003). We acknowledge Dr. Nadica Abazović for measurements of diffuse reflectance and valuable comments, Prof. Dr. Ivanka Holclajtner-Antunović and Prof. Dr. Miloš Mojović for helpful advices and materials.

REFERENCES

1. Li, Y.; Hu, Y.; Zhao, Y.; Shi, G.; Deng, L.; Hou, Y.; Qu, L., An Electrochemical Avenue to Green-Luminescent Graphene Quantum Dots as Potential Electron-Acceptors for Photovoltaics. *Adv. Mater.* **2011**, *23*, 776-780.

2. Luo, P. G.; Yang, F.; Yang, S.-T.; Sonkar, S. K.; Yang, L.; Broglie, J. J.; Liu, Y.; Sun, Y.-P., Carbon-based Quantum Dots for Fluorescence Imaging of Cells and Tissues. *RSC Adv.* **2014**, *4*, 10791-10807.

3. Dong, Y. Q.; Li, G. L.; Zhou, N. N.; Wang, R. X.; Chi, Y. W.; Chen, G. N., Graphene Quantum Dot as a Green and Facile Sensor for Free Chlorine in Drinking Water. *Anal. Chem.* **2012**, *84*, 8378-8382.

4. Razmi, H.; Mohammad-Rezaei, R., Graphene Quantum Dots as a New Substrate for Immobilization and Direct Electrochemistry of Glucose Oxidase: Application to Sensitive Glucose Determination. *Biosens. Bioelectron.* **2013**, *41*, 498-504.

5. Sheng, W. D.; Korkusinski, M.; Guclu, A. D.; Zielinski, M.; Potasz, P.; Kadantsev, E. S.; Voznyy, O.; Hawrylak, P., Electronic and Optical Properties of Semiconductor and Graphene Quantum Dots. *Front. Phys.* **2012**, *7*, 328-352.

6. Molitor, F.; Guttinger, J.; Stampfer, C.; Droscher, S.; Jacobsen, A.; Ihn, T.; Ensslin, K., Electronic Properties of Graphene Nanostructures. *J. Phys.: Condens. Matter* **2011**, *23*, 243201.

7. Pan, D. Y.; Zhang, J. C.; Li, Z.; Wu, M. H., Hydrothermal Route for Cutting Graphene Sheets into Blue-Luminescent Graphene Quantum Dots. *Adv. Mater*. **2010**, *22*, 734-738.

8. Zhang, Z. P.; Zhang, J.; Chen, N.; Qu, L. T., Graphene Quantum Dots: an Emerging Material for Energy-related Applications and Beyond. *Energy Environ. Sci.* **2012**, *5*, 8869-8890.

9. Lu, J. J.; Yan, M.; Ge, L.; Ge, S. G.; Wang, S. W.; Yan, J. X.; Yu, J. H., Electrochemiluminescence of Blue-luminescent Graphene Quantum Dots and its Application in Ultrasensitive Aptasensor for Adenosine Triphosphate Detection. *Biosens. Bioelectron*. **2013**, *47*, 271-277.

10. Qu, D.; Zheng, M.; Du, P.; Zhou, Y.; Zhang, L. G.; Li, D.; Tan, H. Q.; Zhao, Z.; Xie, Z. G.; Sun, Z. C., Highly Luminescent S, N Co-doped Graphene Quantum Dots with Broad Visible Absorption Bands for Visible Light Photocatalysts. *Nanoscale* **2013**, *5*, 12272-12277.

11. Wang, S.; Chen, Z.-G.; Cole, I.; Li, Q., Structural Evolution of Graphene Quantum Dots during Thermal Decomposition of Citric Acid and the Corresponding Photoluminescence. *Carbon* **2015**, *82*, 304-313.

12. Wu, X.; Tian, F.; Wang, W. X.; Chen, J.; Wu, M.; Zhao, J. X., Fabrication of Highly Fluorescent Graphene Quantum Dots using L-glutamic Acid for in Vitro/in Vivo Imaging and Sensing. *J. Mater. Chem. C* **2013**, *1*, 4676-4684.

13. Ananthanarayanan, A.; Wang, Y.; Routh, P.; Sk, M. A.; Than, A.; Lin, M.; Zhang, J.; Chen, J.; Sun, H.; Chen, P., Nitrogen and Phosphorus Co-doped Graphene Quantum Dots: Synthesis from Adenosine Triphosphate, Optical Properties, and Cellular Imaging. *Nanoscale* **2015**, *7*, 8159-8165.

14. Liu, R. L.; Wu, D. Q.; Feng, X. L.; Mullen, K., Bottom-Up Fabrication of Photoluminescent Graphene Quantum Dots with Uniform Morphology. *J. Am. Chem. Soc.* **2011**, *133*, 15221-15223.

15. Feng, Q.; Cao, Q. Q.; Li, M.; Liu, F. C.; Tang, N. J.; Du, Y. W., Synthesis and Photoluminescence of Fluorinated Graphene Quantum Dots. *Appl. Phys. Lett.* **2013**, *102*, 013111.

16. Lin, L. X.; Zhang, S. W., Creating High Yield Water Soluble Luminescent Graphene Quantum Dots via Exfoliating and Disintegrating Carbon Nanotubes and Graphite Flakes. *Chem. Commun.* **2012**, *48*, 10177-10179.

17. Shinde, D. B.; Pillai, V. K., Electrochemical Preparation of Luminescent Graphene Quantum Dots from Multiwalled Carbon Nanotubes. *Chem. - Eur. J.* **2012**, *18*, 12522-12528.

18. Chua, C. K.; Sofer, Z.; Šimek, P.; Jankovský, O.; Klímová, K.; Bakardjieva, S.; Hrdličková Kučková, Š.; Pumera, M., Synthesis of Strongly Fluorescent Graphene Quantum Dots by Cage-Opening Buckminsterfullerene. *ACS Nano* **2015**, *9*, 2548-2555.

19. Tan, X.; Li, Y.; Li, X.; Zhou, S.; Fan, L.; Yang, S., Electrochemical Synthesis of Small-sized Red Fluorescent Graphene Quantum Dots as a Bioimaging Platform. *Chem. Commun.* **2015**, *51*, 2544-2546.

20. Chen, X.; Li, C.; Gratzel, M.; Kostecki, R.; Mao, S. S., Nanomaterials for renewable energy production and storage. *Chem. Soc. Rev*. **2012**, *41*, 7909-7937.

21. Zhang, M.; Bai, L. L.; Shang, W. H.; Xie, W. J.; Ma, H.; Fu, Y. Y.; Fang, D. C.; Sun, H.; Fan, L. Z.; Han, M.; Liu, C. M.; Yang, S. H., Facile Synthesis of Water-soluble, Highly Fluorescent Graphene Quantum Dots as a Robust Biological Label for Stem Cells. *J. Mater. Chem.* **2012**, *22*, 7461-7467.

22. Ye, R. Q.; Xiang, C. S.; Lin, J.; Peng, Z. W.; Huang, K. W.; Yan, Z.; Cook, N. P.; Samuel, E. L. G.; Hwang, C. C.; Ruan, G. D.; Ceriotti, G.; Raji, A. R. O.; Marti, A. A.; Tour, J. M., Coal as an Abundant Source of Graphene Quantum Dots. *Nat. Commun.* **2013**, *4*, 2934.

23. Sun, Y. Q.; Wang, S. Q.; Li, C.; Luo, P. H.; Tao, L.; Wei, Y.; Shi, G. Q., Large Scale Preparation of Graphene Quantum Dots from Graphite with Tunable Fluorescence Properties. *Phys. Chem. Chem. Phys.* **2013**, *15*, 9907-9913.

24. Nurunnabi, M.; Khatun, Z.; Nafiujjaman, M.; Lee, D. G.; Lee, Y. K., Surface Coating of Graphene Quantum Dots Using Mussel-Inspired Polydopamine for Biomedical Optical Imaging. *ACS Appl. Mater. Interfaces* **2013**, *5*, 8246-8253.

25. Zheng, X. T.; He, H. L.; Li, C. M., Multifunctional Graphene Quantum Dots-conjugated Titanate Nanoflowers for Fluorescence-trackable Targeted Drug Delivery. *RSC Adv.* **2013**, *3*, 24853-24857.

26. Markovic, Z. M.; Ristic, B. Z.; Arsikin, K. M.; Klisic, D. G.; Harhaji-Trajkovic, L. M.; Todorovic-Markovic, B. M.; Kepic, D. P.; Kravic-Stevovic, T. K.; Jovanovic, S. P.; Milenkovic, M. M.; Milivojevic, D. D.; Bumbasirevic, V. Z.; Dramicanin, M. D.; Trajkovic, V. S., Graphene Quantum Dots as Autophagy-inducing Photodynamic Agents. *Biomaterials* **2012**, *33*, 7084-7092.

27. Ristic, B. Z.; Milenkovic, M. M.; Dakic, I. R.; Todorovic-Markovic, B. M.; Milosavljevic, M. S.; Budimir, M. D.; Paunovic, V. G.; Dramicanin, M. D.; Markovic, Z. M.; Trajkovic, V. S., Photodynamic Antibacterial Effect of Graphene Quantum Dots. *Biomaterials* **2014**, *35*, 4428-35.

28. Ge, J.; Lan, M.; Zhou, B.; Liu, W.; Guo, L.; Wang, H.; Jia, Q.; Niu, G.; Huang, X.; Zhou, H.; Meng, X.; Wang, P.; Lee, C.-S.; Zhang, W.; Han, X., A Graphene Quantum Dot Photodynamic Therapy Agent with High Singlet Oxygen Generation. *Nat. Commun*. **2014**, *5*, 4596.

29. Dolmans, D. E. J. G. J.; Fukumura, D.; Jain, R. K., Photodynamic Therapy for Cancer. *Nat. Rev. Cancer* **2003**, *3*, 380-387.

30. Hamblin, M. R.; Hasan, T., Photodynamic Therapy: a New Antimicrobial Approach to Infectious Disease? *Photochem. Photobiol. Sci.* **2004**, *3*, 436-50.

31. Jovanovic, S. P.; Markovic, Z. M.; Kleut, D. N.; Tosic, D. D.; Kepic, D. P.; Cincovic, M. T. M.; Antunovic, I. D. H.; Markovic, B. M. T., Covalent Modification of Single Wall Carbon Nanotubes Upon Gamma Irradiation in Aqueous Media. *Hem. Ind.* **2011**, *65*, 479-487.

32. Kleut, D.; Jovanovic, S.; Markovic, Z.; Kepic, D.; Tosic, D.; Romcevic, N.; Marinovic-Cincovic, M.; Dramicanin, M.; Holclajtner-Antunovic, I.; Pavlovic, V.; Drazic, G.; Milosavljevic, M.; Markovic, B. T., Comparison of Structural Properties of Pristine and Gamma Irradiated Single-wall Carbon Nanotubes: Effects of Medium and Irradiation Dose. *Mater. Charact.* **2012**, *72*, 37-45.

33. Tosic, D.; Markovic, Z.; Dramicanin, M.; Antunovic, I. H.; Jovanovic, S.; Milosavljevic, M.; Pantic, J.; Markovic, B. T., Gamma Ray Assisted Fabrication of Fluorescent Oligographene Nanoribbons. *Mater. Res. Bull*. **2012**, *47*, 1996-2000.

34. Kleut, D. N.; Markovi, Z. M.; Babic, B. M.; Antunovic, I. D. H.; Milosavljevic, M. S.; Dramicanin, M. D.; Markovic, B. M. T., Raman Spectroscopy Study of Carbon-doped Resorcinol-formaldehyde Thin Films. *Phys. Scr*., *T* **2013**, 157.

35. Feng, Y. Q.; Zhao, J. P.; Yan, X. B.; Tang, F. L.; Xue, Q. J., Enhancement in the Fluorescence of Graphene Quantum Dots by Hydrazine Hydrate Reduction. *Carbon* **2014**, *66*, 334-339.

36. Jovanović, S. P.; Marković, Z. M.; Kleut, D. N.; Dramićanin, M. D.; Holclajtner-Antunović, I. D.; Milosavljević, M. S.; La Parola, V.; Syrgiannis, Z.; Todorović Marković, B. M., Structural Analysis of Single Wall Carbon Nanotubes Exposed to Oxidation and Reduction Conditions in the Course of Gamma Irradiation. *J. Phys. Chem. C* **2014**, *118*, 16147-16155.

37. Li, H. T.; He, X. D.; Kang, Z. H.; Huang, H.; Liu, Y.; Liu, J. L.; Lian, S. Y.; Tsang, C. H. A.; Yang, X. B.; Lee, S. T., Water-Soluble Fluorescent Carbon Quantum Dots and Photocatalyst Design. *Angew. Chem., Int. Edit*. **2010**, *49*, 4430-4434.

38. Ding, Z.; Hao, Z.; Meng, B.; Xie, Z.; Liu, J.; Dai, L., Few-layered Graphene Quantum Dots as Efficient Hole-extraction Layer for High-performance Polymer Solar Cells. *Nano Energy* **2015**, *15*, 186-192.

39. Kleut, D. N.; Marković, Z. M.; Antunović, I. D. H.; Dramićanin, M. D.; Kepić, D. P.; Marković, B. M. T., Gamma Ray-assisted Irradiation of Few-layer Graphene Films: a Raman Spectroscopy Study. *Phys. Scr., T* **2014** (T162), 014025.

40. Kwon, W.; Rhee, S. W., Facile Synthesis of Graphitic Carbon Quantum Dots with Size Tunability and Uniformity using Reverse Micelles. *Chem. Commun*. **2012**, *48*, 5256-5258.

41. Yang, F.; Zhao, M. L.; Zheng, B. Z.; Xiao, D.; Wu, L.; Guo, Y., Influence of pH on the Fluorescence Properties of Graphene Quantum Dots using Ozonation Pre-oxide Hydrothermal Synthesis. *J. Mater. Chem*. **2012**, *22*, 25471-25479.

42. Eschemann, T. O.; Lamme, W. S.; Manchester, R. L.; Parmentier, T. E.; Cognigni, A.; Ronning, M.; de Jong, K. P., Effect of Support Surface Treatment on the Synthesis, Structure, and Performance of Co/CNT Fischer–Tropsch Catalysts. *J. Catal.* **2015**, *328*, 130-138.

43. Bao, L.; Zhang, Z. L.; Tian, Z. Q.; Zhang, L.; Liu, C.; Lin, Y.; Qi, B.; Pang, D. W., Electrochemical Tuning of Luminescent Carbon Nanodots: from Preparation to Luminescence Mechanism. *Adv. Mater.* **2011**, *23*, 5801-5806.

44. Peng, J.; Gao, W.; Gupta, B. K.; Liu, Z.; Romero-Aburto, R.; Ge, L. H.; Song, L.; Alemany, L. B.; Zhan, X. B.; Gao, G. H.; Vithayathil, S. A.; Kaipparettu, B. A.; Marti, A. A.;

Hayashi, T.; Zhu, J. J.; Ajayan, P. M., Graphene Quantum Dots Derived from Carbon Fibers. *Nano Lett*. **2012**, *12*, 844-849.

45. Yan, X.; Li, B. S.; Cui, X.; Wei, Q. S.; Tajima, K.; Li, L. S., Independent Tuning of the Band Gap and Redox Potential of Graphene Quantum Dots. *J. Phys. Chem. Lett*. **2011**, *2*, 1119-1124.

46. Shi, H. Q.; Barnard, A. S.; Snook, I. K., Site-dependent Stability and Electronic Structure of Single Vacancy Point Defects in Hexagonal Graphene Nano-flakes. *Phys. Chem. Chem. Phys*. **2013**, *15*, 4897-4905.

47. Zhu, S. J.; Zhang, J. H.; Tang, S. J.; Qiao, C. Y.; Wang, L.; Wang, H. Y.; Liu, X.; Li, B.; Li, Y. F.; Yu, W. L.; Wang, X. F.; Sun, H. C.; Yang, B., Surface Chemistry Routes to Modulate the Photoluminescence of Graphene Quantum Dots: From Fluorescence Mechanism to Up-Conversion Bioimaging Applications. *Adv. Funct. Mater*. **2012**, *22*, 4732-4740.

48. Xu, Q. F.; Zhou, Q.; Hua, Z.; Xue, Q.; Zhang, C. F.; Wang, X. Y.; Pan, D. Y.; Xiao, M., Single-Particle Spectroscopic Measurements of Fluorescent Graphene Quantum Dots. *ACS Nano* **2013**, *7*, 10654-10661.

49. Qu, D.; Zheng, M.; Zhang, L.; Zhao, H.; Xie, Z.; Jing, X.; Haddad, R. E.; Fan, H.; Sun, Z., Formation Mechanism and Optimization of Highly Luminescent N-doped Graphene Quantum Dots. *Sci. Rep*. **2014**, *4*, 5294.

50. Velo-Gala, I.; Lopez-Penalver, J. J.; Sanchez-Polo, M.; Rivera-Utrilla, J., Surface Modifications of Activated Carbon by Gamma Irradiation. *Carbon* **2014**, *67*, 236-249.

51. Luan, C. Y.; Vaneski, A.; Susha, A. S.; Xu, X. Q.; Wang, H. E.; Chen, X.; Xu, J.; Zhang, W. J.; Lee, C. S.; Rogach, A. L.; Zapien, J. A., Facile Solution Growth of Vertically Aligned

ZnO Nanorods Sensitized with Aqueous CdS and CdSe Quantum Dots for Photovoltaic Applications. *Nanoscale Res. Lett.* **2011**, *6*, 1-8.

52. Lopez, R.; Gomez, R., Band-gap Energy Estimation from Diffuse Reflectance Measurements on Sol-gel and Commercial TiO2: a Comparative Study. *J. Sol-Gel Sci. Technol*. **2012**, *61*, 1−7.

53. Barklie, R. C., Characterisation of Defects in Amorphous Carbon by Electron Paramagnetic Resonance. *Diamond Relat. Mater*. **2001**, *10*, 174−181.

54. Wu, T. M.; Chang, H. L.; Lin, Y. W., Synthesis and Characterization of Conductive Polypyrrole with Improved Conductivity and Processability. *Polym. Int.* **2009**, *58*, 1065−1070.

55. Gupta, S.; Luthra, V.; Singh, R., Electrical Transport and EPR investigations: A Comparative Study for D.C. Conduction Mechanism in Monovalent and Multivalent Ions Doped Polyaniline. *Bull. Mater. Sci.* **2012**, *35*, 787−794.

56. Hsu, F.-H.; Wu, T.-M., In Situ Synthesis and Characterization of Conductive Polypyrrole/graphene Composites with Improved Solubility and Conductivity. *Synth. Met*. **2012**, *162*, 682−687.

57. Rao, S. S.; Stesmans, A.; Kosynkin, D. V.; Higginbotham, A.; Tour, J. M., Paramagnetic Centers in Graphene Nanoribbons Prepared from Longitudinal Unzipping of Carbon Nanotubes. *New J. Phys*. **2011**, *13*, 113004−1−9.

58. Shibayama, Y.; Sato, H.; Enoki, T.; Endo, M., Disordered Magnetism at the Metal-Insulator Threshold in Nano-Graphite-Based Carbon Materials. *Phys. Rev. Lett*. **2000**, *84*, 1744−1747.

59. Lion, Y.; Delmelle, M.; Van De Vorst, A., New Method of Detecting Singlet Oxygen Production. *Nature* **1976**, *263*, 442−443.

60. Moan, J.; Wold, E., Detection of Singlet Oxygen Production by ESR. *Nature* **1979**, *279*, 450-451.

61. Adarsh, N.; Avirah, R. R.; Ramaiah D., Tuning Photosensitized Singlet Oxygen Generation Efficiency of Novel Aza-BODIPY Dyes. *Org. Lett.* **2010**, *12*, 5720–5723.

62. Awuah, S. G.; Polreis, J.; Biradar, V.; You, Y., Singlet Oxygen Generation by Novel NIR BODIPY Dyes. *Org. Lett.* **2011**, *13*, 3884–3887.

63. Li, W.; Li, L.; Xiao, H.; Qi, R.; Huang, Y.; Xie, Z.; Jing, X.; Zhang, H., Iodo BODIPY: a Visible-light-driven, Highly Efficient and Photostabile Metal-free Oragnic Photocatalyst. *RSC Adv.* **2013**, *3*, 13417–13421.

64. Khan, R.; Idris, M.; Tuncel, D., Synthesis and Investigation of Singlet Oxygen Production Efficiency of Photosensitizers Based on Meso-phenyl-2,5-thienylene Linked Porphyrin Oligomers and Polymers. *Org. Biomol. Chem*. **2015**, *13*, 10496–10504.

Table of Contents Graphic and Synopsis

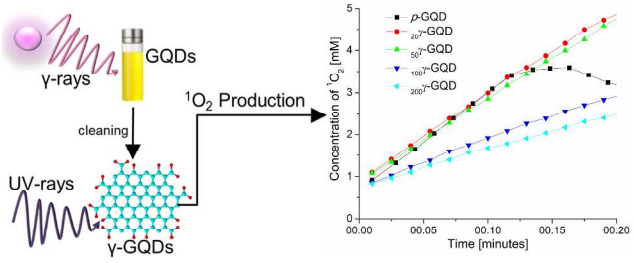

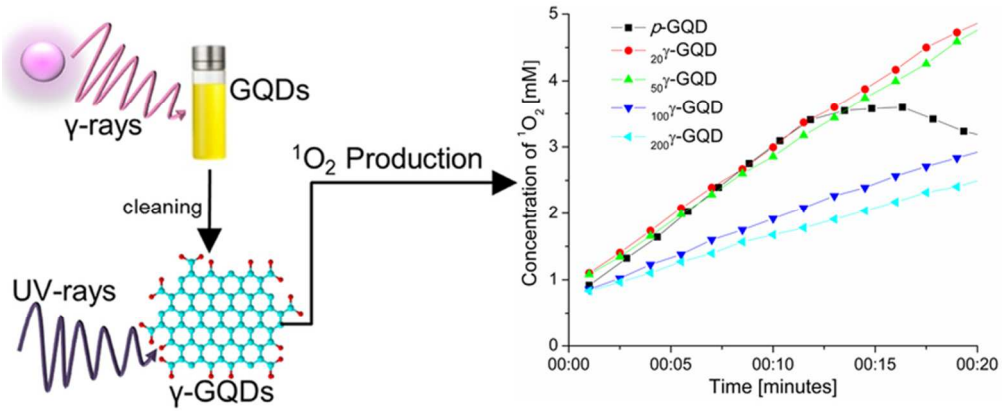

Table of Contents Graphic and Synopsis
35x15mm (600 x 600 DPI)

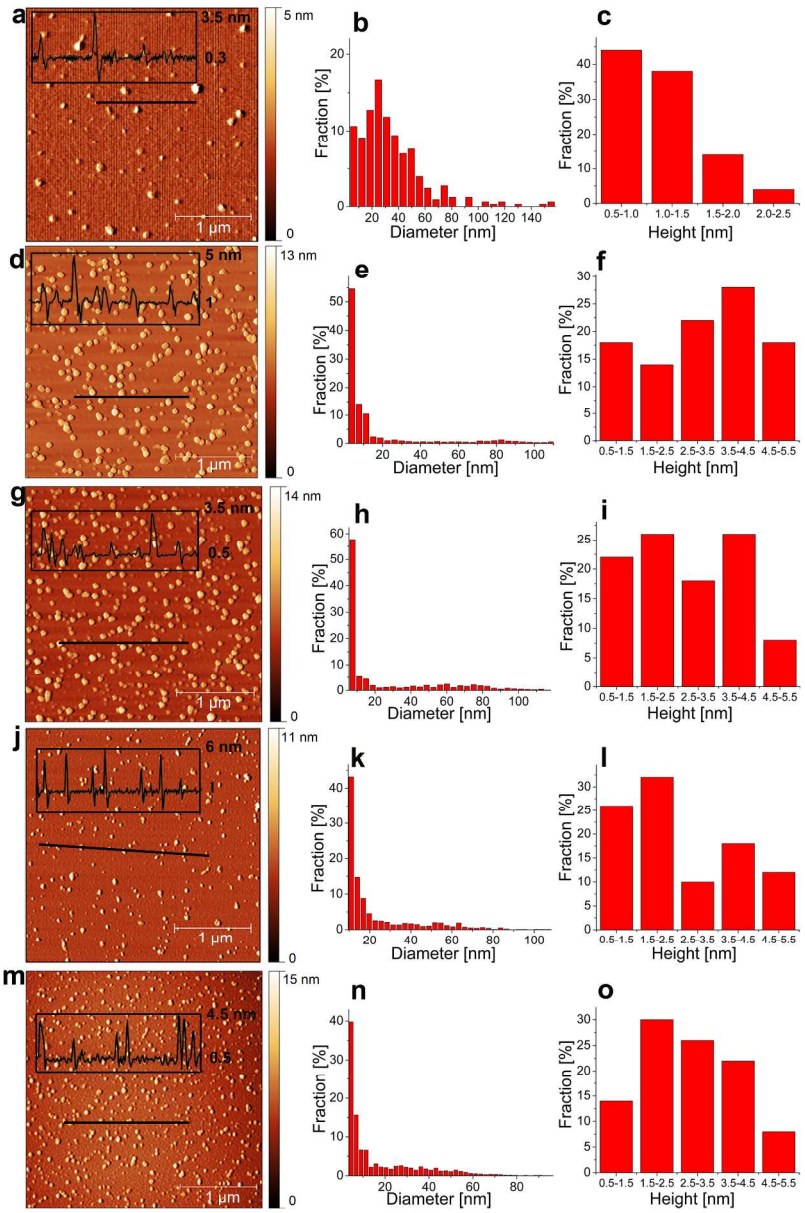

Figure 1
225x340mm (300 x 300 DPI)

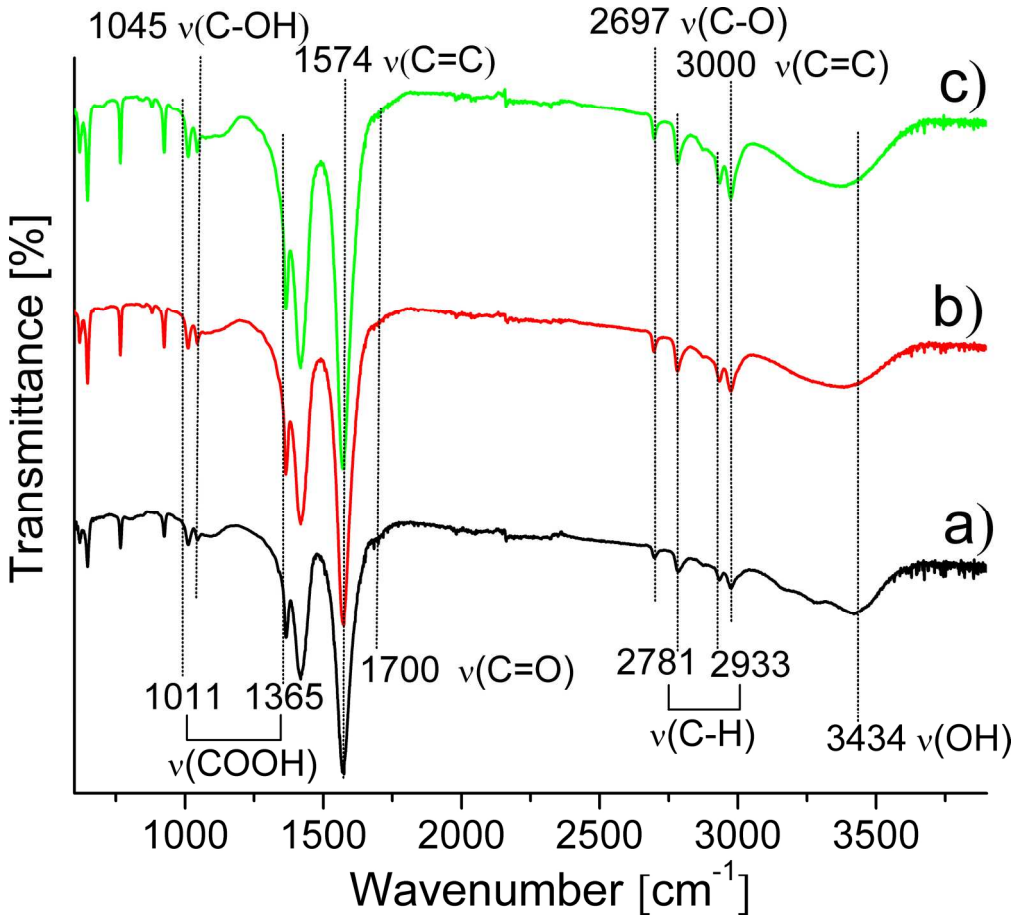

Figure 2
189x171mm (300 x 300 DPI)

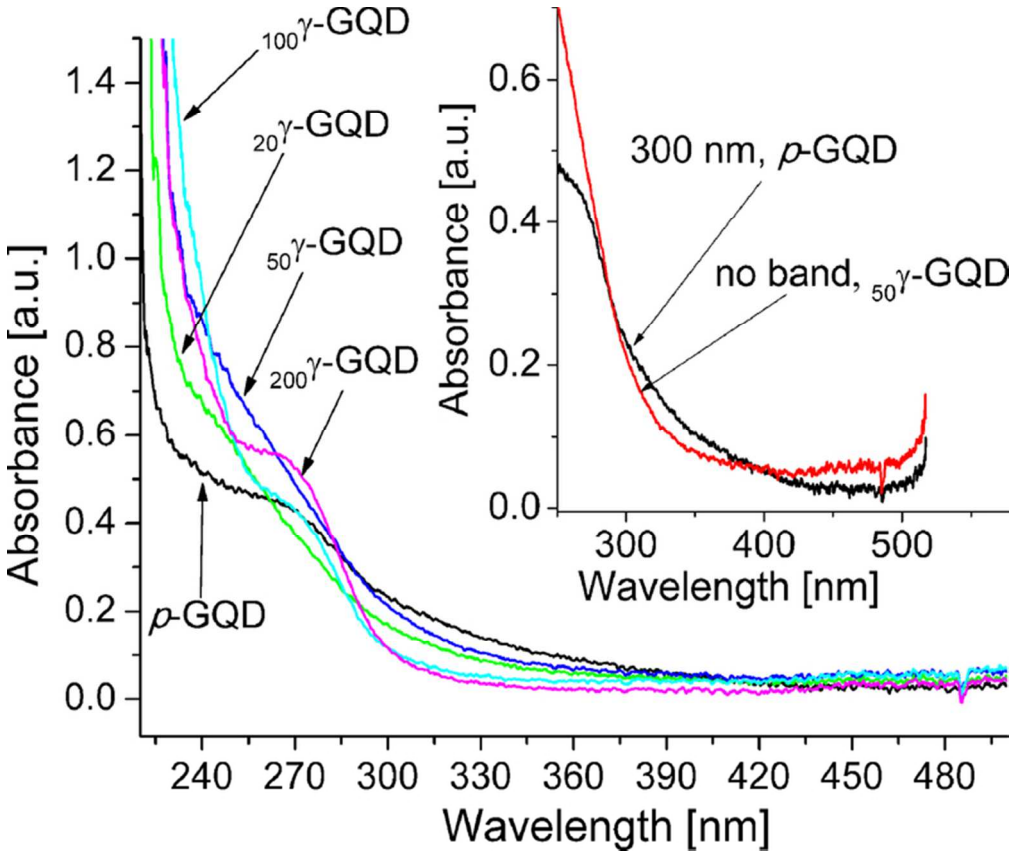

Figure 3
67x56mm (300 x 300 DPI)

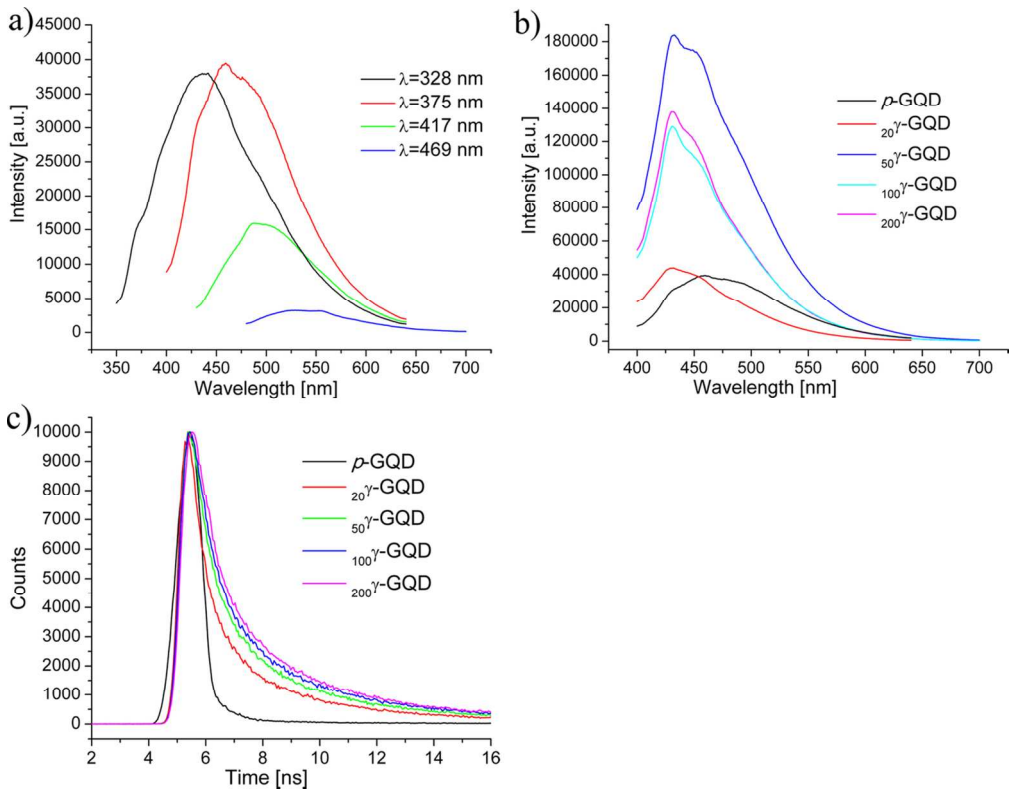

Figure 4
119x93mm (300 x 300 DPI)

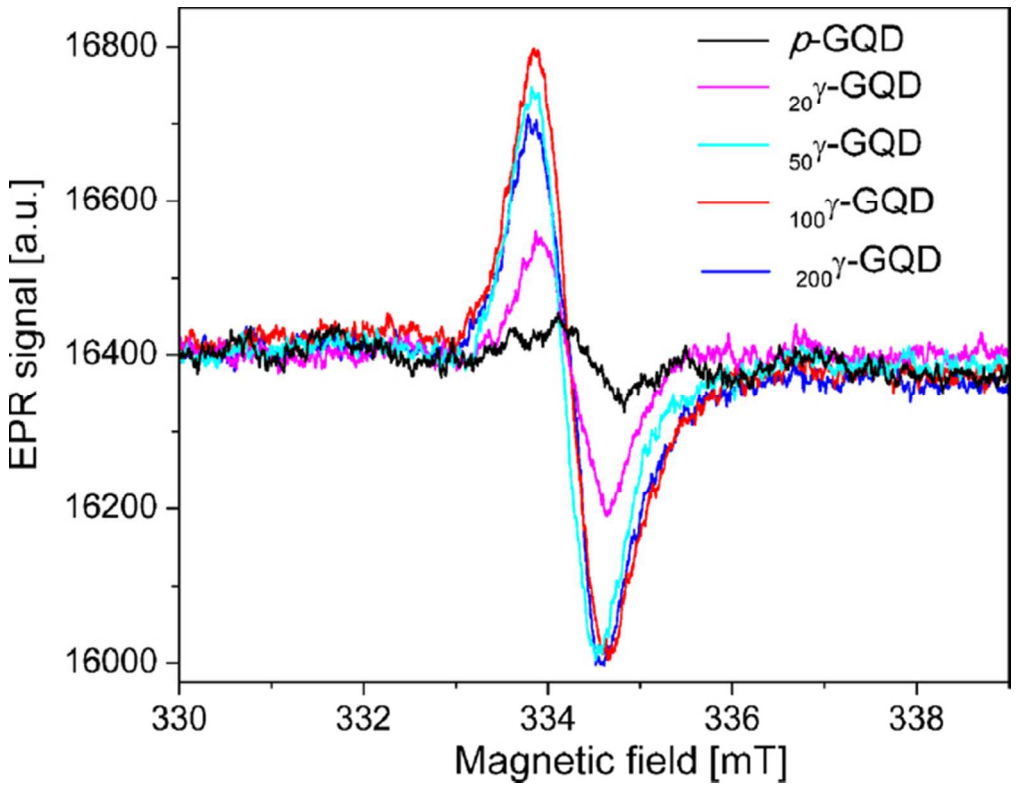

Figure 5
58x45mm (300 x 300 DPI)

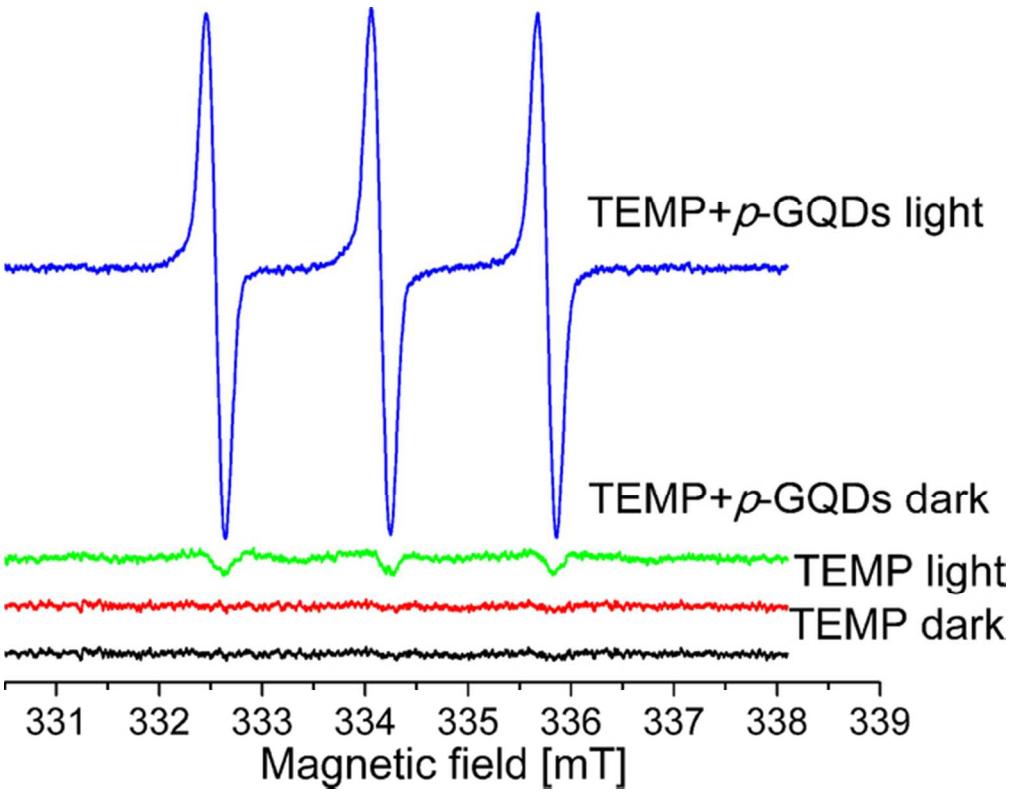

Figure 6
58x45mm (300 x 300 DPI)

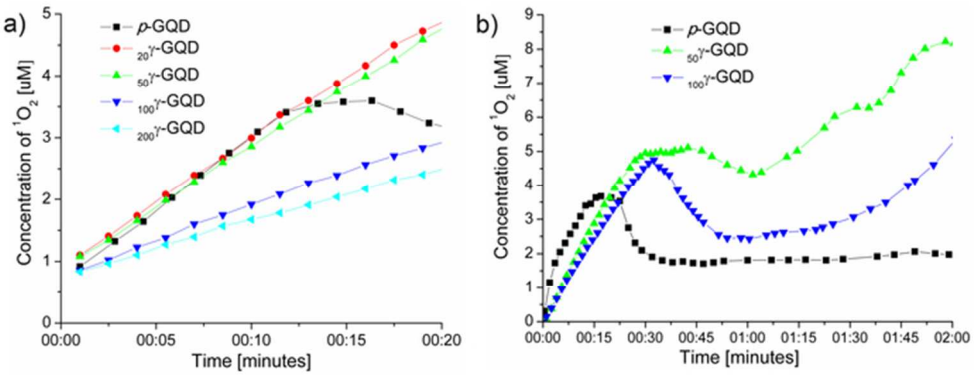

Figure 7
59x23mm (300 x 300 DPI)

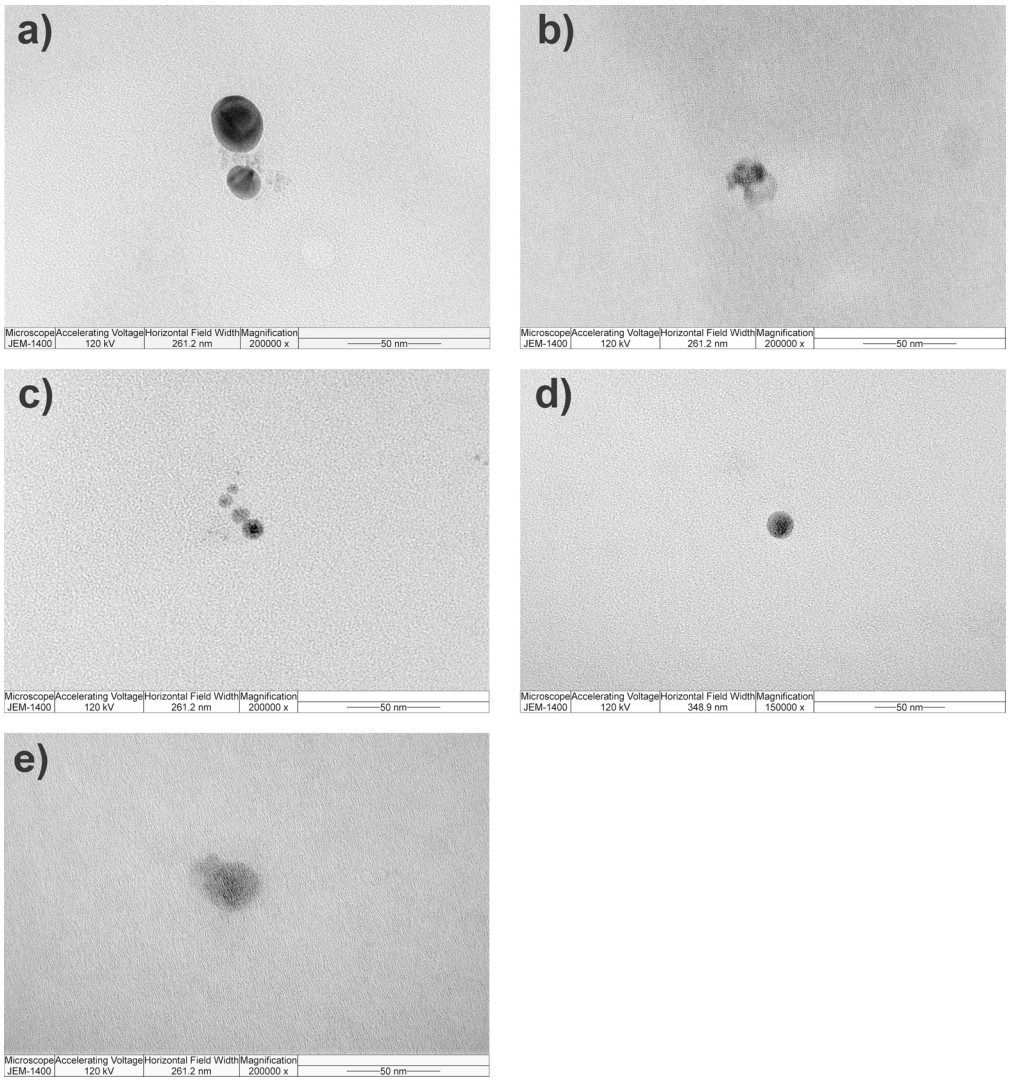

Figure S1
160x171mm (300 x 300 DPI)

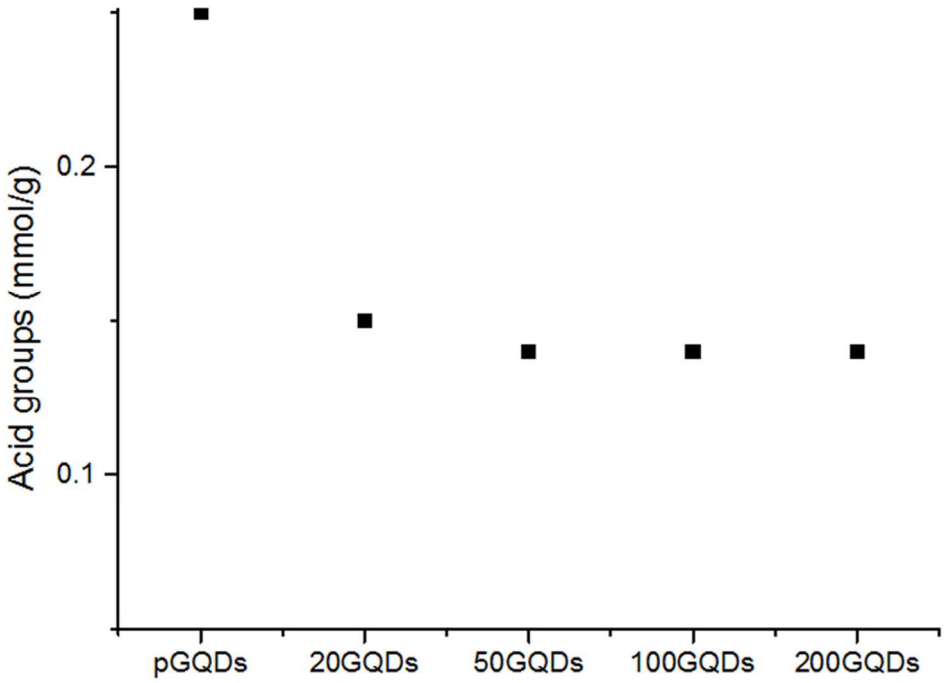

Figure S2
80x59mm (300 x 300 DPI)

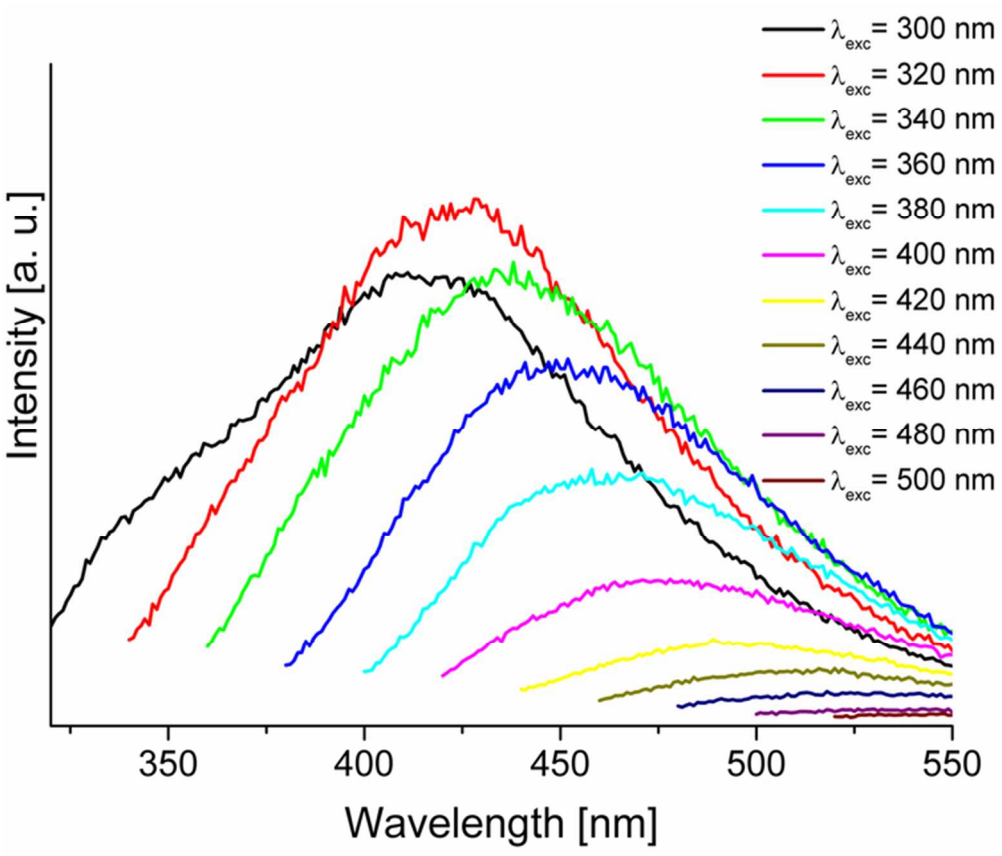

Figure S3
63x54mm (300 x 300 DPI)

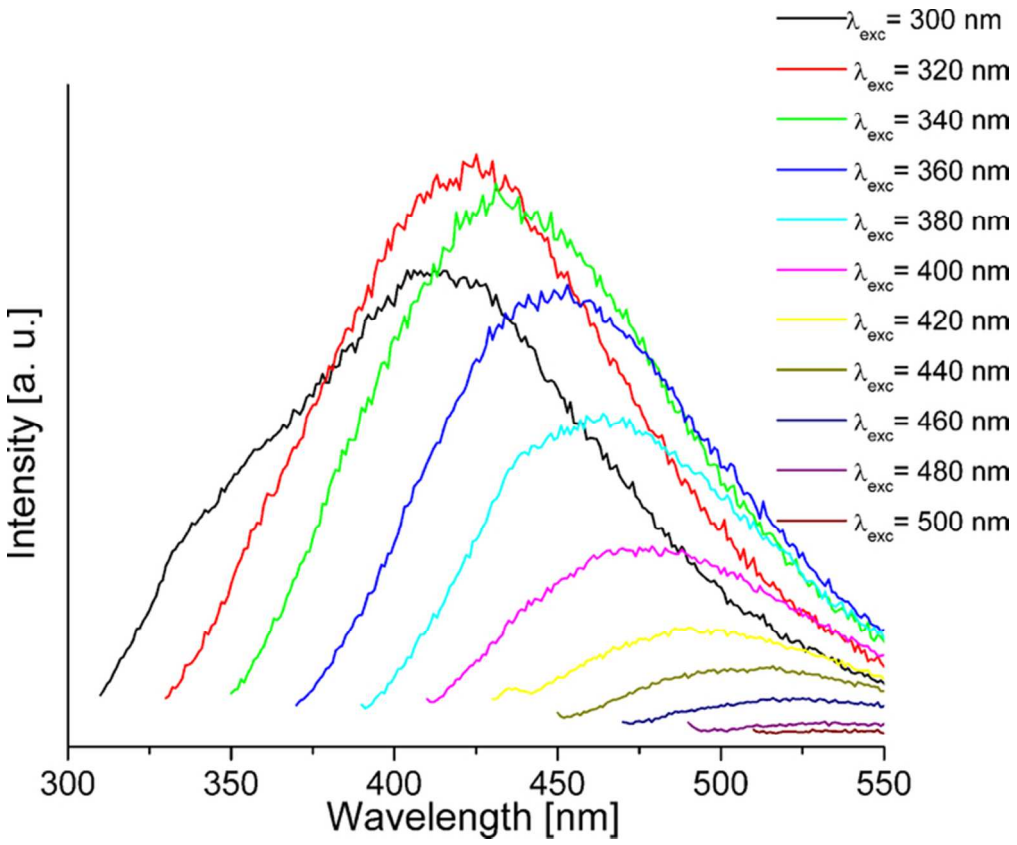

Figure S4
62x51mm (300 x 300 DPI)

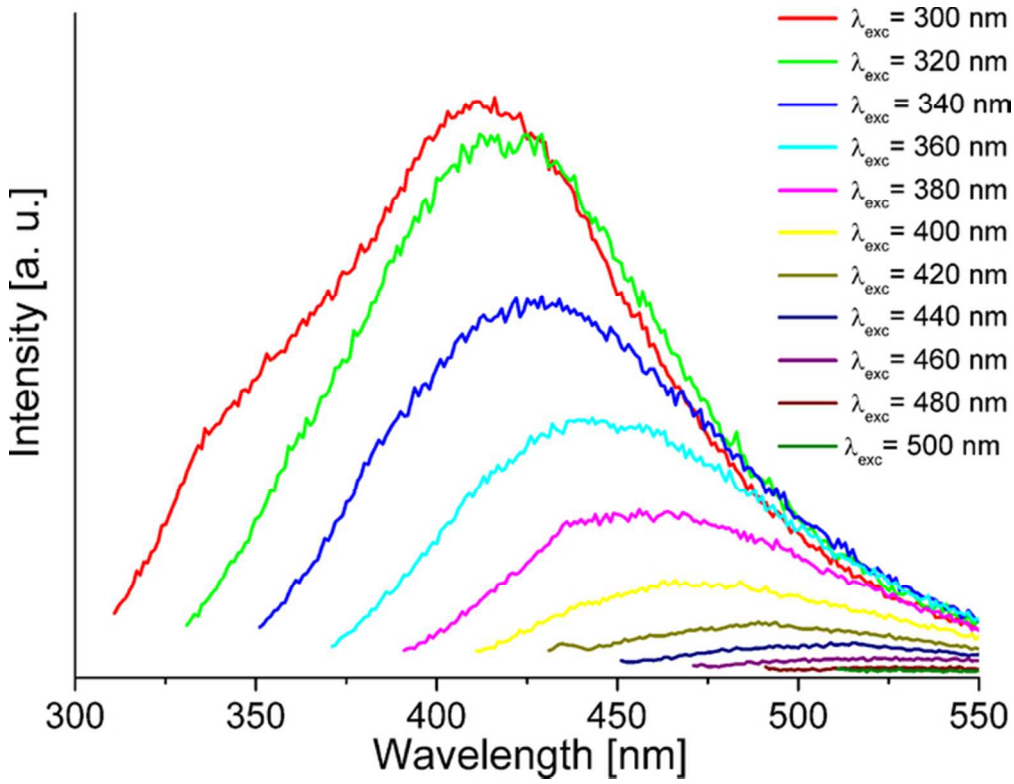

Figure S5
57x44mm (300 x 300 DPI)

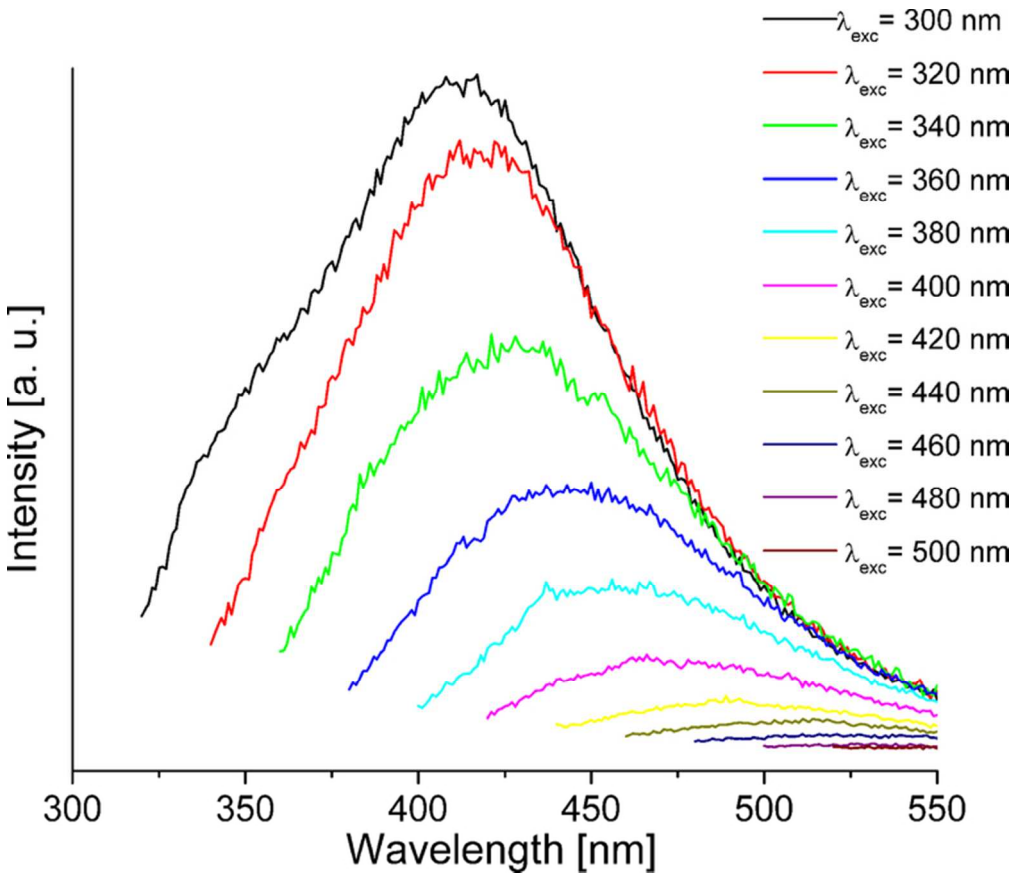

Figure S6
64x55mm (300 x 300 DPI)

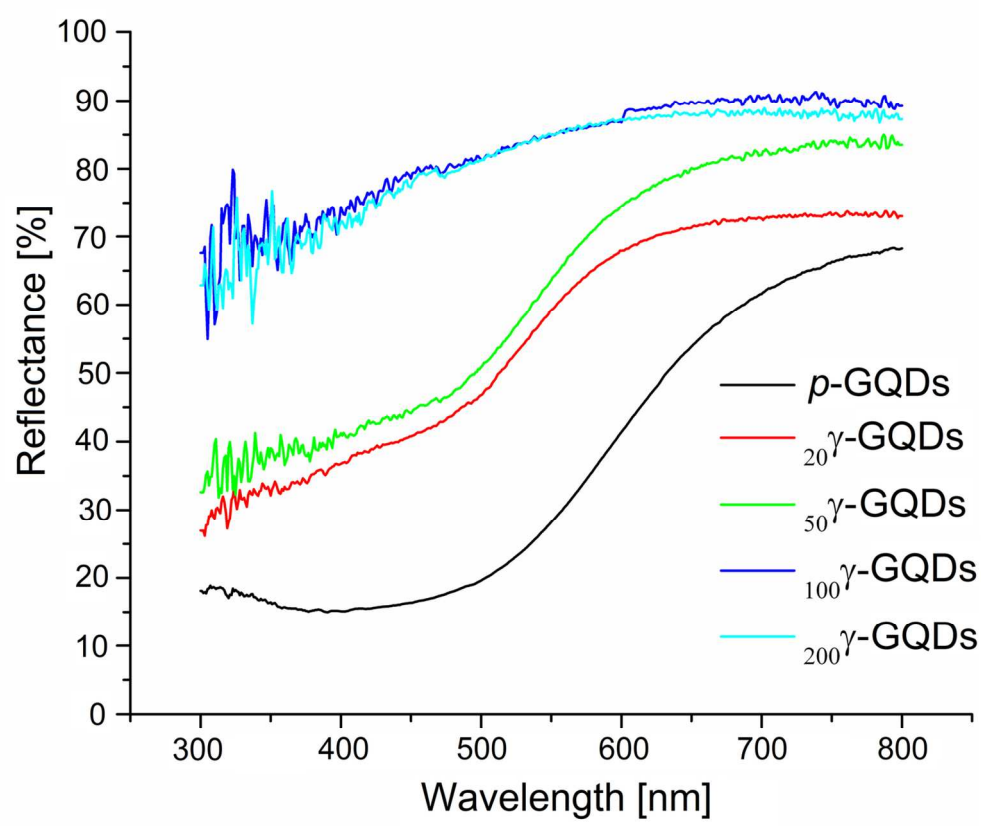

Figure S7
66x55mm (600 x 600 DPI)

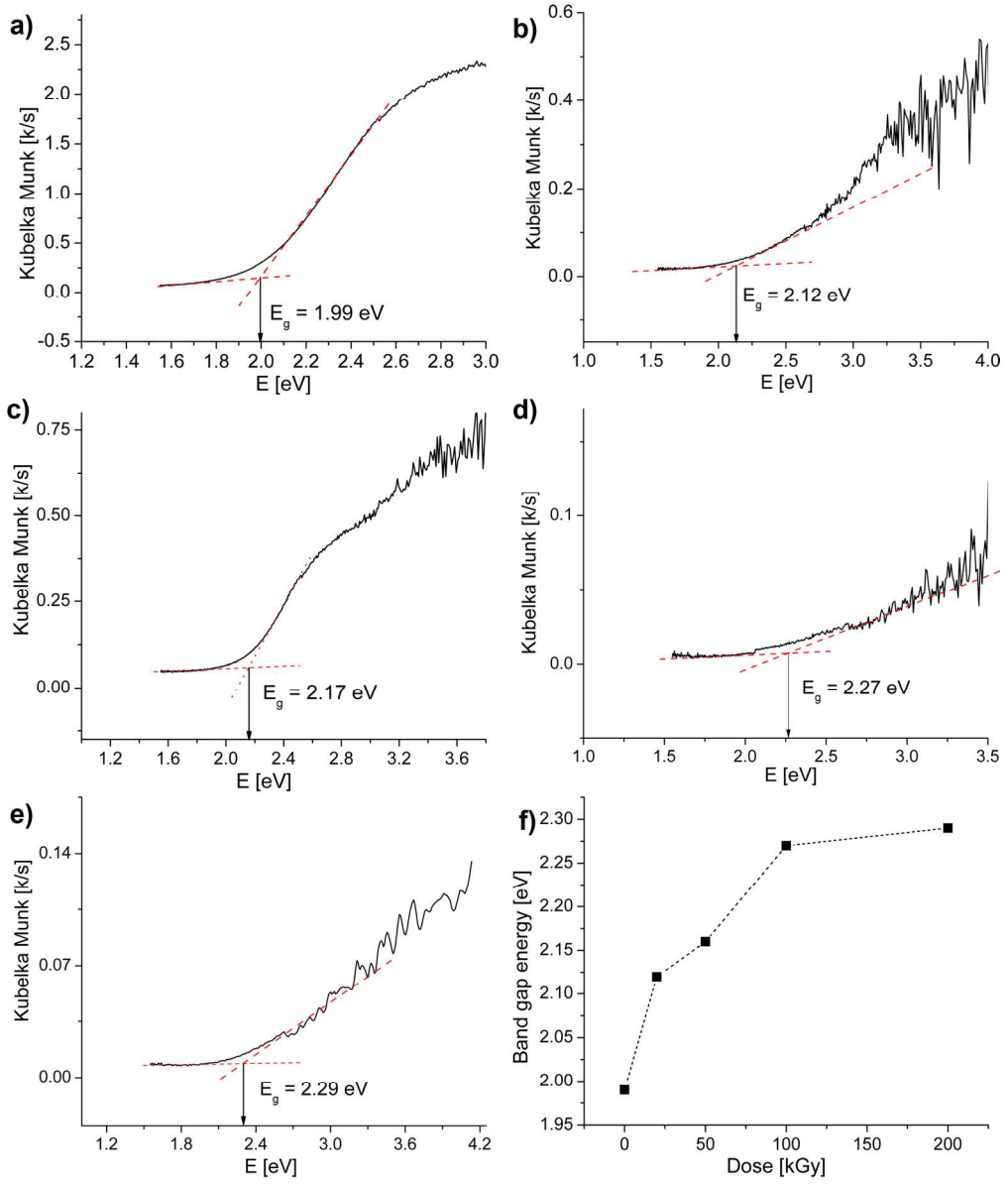

Figure S8
173x206mm (300 x 300 DPI)

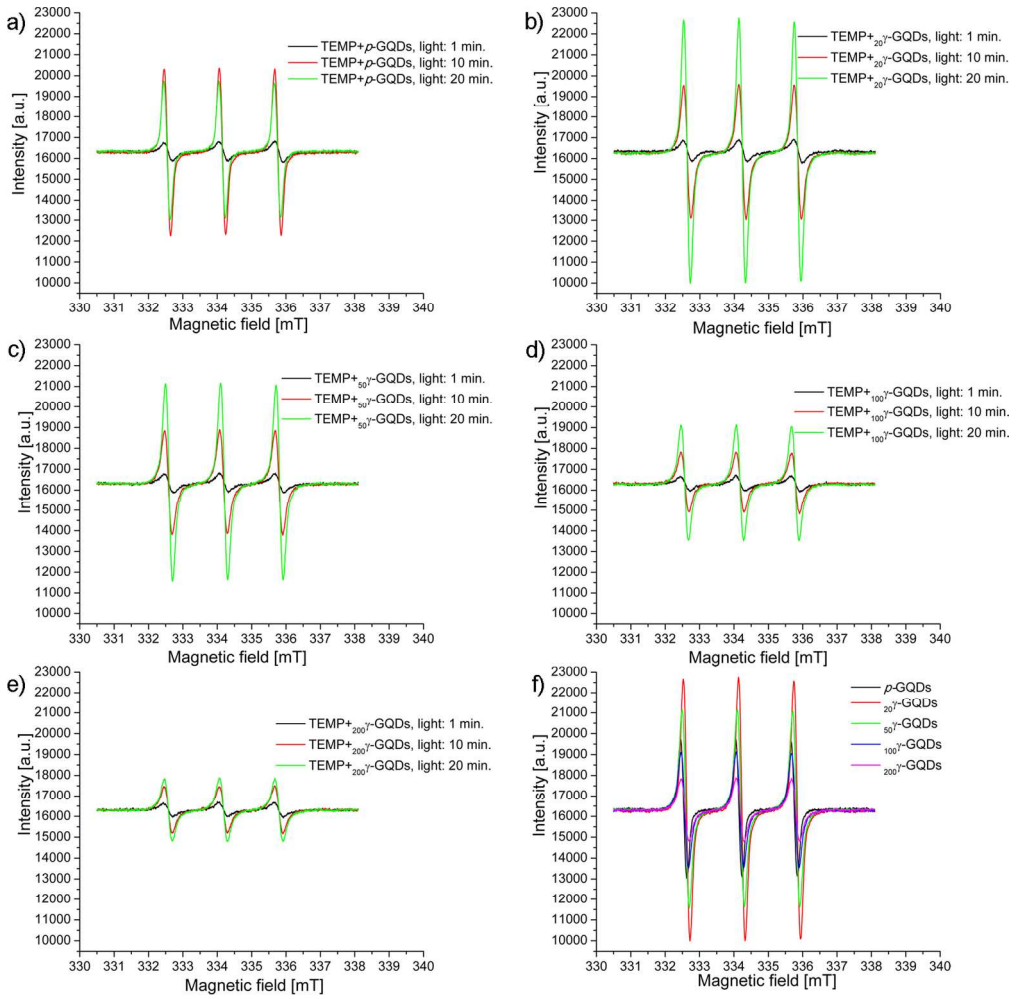

Figure S9
150x147mm (300 x 300 DPI)

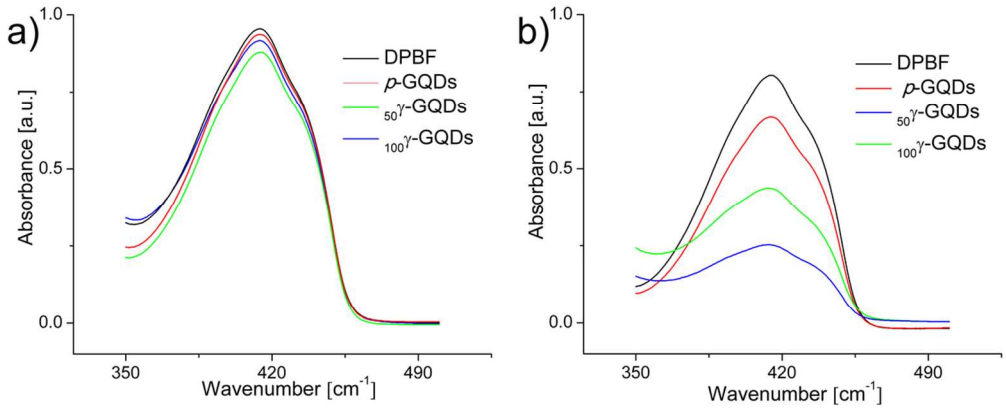

Figure S10
110x44mm (300 x 300 DPI)